

**OPTICAL INVESTIGATION OF  
MOLECULAR BEAM EPITAXY  $\text{Al}_x\text{Ga}_{1-x}\text{N}$  TO  
DETERMINE MATERIAL QUALITY**

THESIS

Judith L. McFall, First Lieutenant, USAF

AFIT/GMS/ENP/00M-01

**DEPARTMENT OF THE AIR FORCE  
AIR UNIVERSITY**

**AIR FORCE INSTITUTE OF TECHNOLOGY**

---

**Wright-Patterson Air Force Base, Ohio**

APPROVED FOR PUBLIC RELEASE; DISTRIBUTION UNLIMITED.

**DTIC QUALITY INSURED**

20001113 028

The views expressed in this thesis are those of the author and do not reflect the official policy or position of the Department of Defense or the U. S. Government.

AFIT/GMS/ENP/00M-01

OPTICAL INVESTIGATION OF MOLECULAR BEAM EPITAXY  $\text{Al}_x\text{Ga}_{1-x}\text{N}$  TO  
DETERMINE MATERIAL QUALITY

THESIS

Presented to the Faculty

Department of Engineering Physics

Graduate School of Engineering and Management

Air Force Institute of Technology

Air University

Air Education and Training Command

In Partial Fulfillment of the Requirements for the

Degree of Master of Science in Material Science and Engineering

Judith L. McFall, B.S.

First Lieutenant, USAF

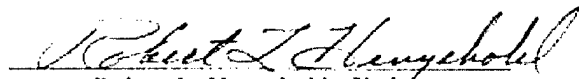
March 2000

APPROVED FOR PUBLIC RELEASE; DISTRIBUTION UNLIMITED.

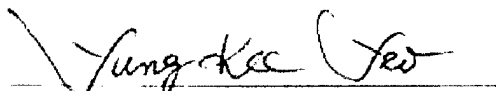
OPTICAL INVESTIGATION OF MOLECULAR BEAM EPITAXY  $\text{Al}_x\text{Ga}_{1-x}\text{N}$  TO  
DETERMINE MATERIAL QUALITY

Judith L. McFall, B.S.  
First Lieutenant, USAF

Approved:

  
Robert L. Hengehold (Chairman)

6 March 2000  
date

  
Yung K. Yeo (Member)

6 March 2000  
date

  
Joe E. Van Nostrand (Member)

6 March 00  
date

## Acknowledgments

Obtaining any degree is not a solitary effort. Thus, I would like to extended to the following a deep appreciation for their patience and aid in this endeavor. First, I would like to thank my thesis advisor, Dr. Robert L. Hengehold, for showing me how to go from the macro to mirco in materials. Also, for his insight into deciphering the spectra of AlGa<sub>N</sub>. Following right behind my thesis advisor, I would like to thank the other two members of my committee, Dr. Yung K. Yeo and Dr. Joe E. Van Nostrand. Both members lent knowledge in understanding the spectra of AlGa<sub>N</sub>. In addition to the spectra interpretation, I would like to thank Joe Van Nostrand and Eric Taylor of the Wright-Patterson Material Laboratory for growing the samples used in this research. As to the running of the experiments, I extended a heart felt thanks to the technicians, especially Greg Smith, who patiently taught and answered my questions on the usage of the equipment and took my photoluminescence data when circumstances prevented me from being able to perform the experiment. Not only did he teach me the equipment but also he kept it running when it would have preferred to walk. Lastly, to my parents, Shirley and David McFall, for without their support in the obtaining my undergraduate degree, none of this would have been possible.

Judith L. McFall

## Table of Contents

Acknowledgments .....	ii
Table of Contents .....	iii
List of Figures .....	v
List of Tables .....	vi
Abstract .....	vii
I. Introduction.....	1
II. Theory.....	4
Optical Absorption .....	4
Luminescence .....	5
Radiative Transitions .....	5
Phonon Replicas .....	10
Laser Penetration.....	11
Electron Penetration .....	11
Molecular Beam Epitaxy.....	12
III. Methodology .....	15
Sample Information .....	15
Molecular Beam Epitaxy.....	16
Sample Preparation and Mounting .....	16
Optical Absorption System Setup.....	17
Cathodoluminescence System Setup .....	17
Photoluminescence System Setup .....	20
IV. Results and Discussion.....	23
Optical Absorption .....	23
Cathodoluminescence .....	26
GaN Standard .....	27
AlGaN Samples .....	29
AlN Buffer Layer .....	38
Photoluminescence .....	43

V. Conclusions and Recommendations .....	49
Conclusion.....	49
Recommendations.....	52
Appendix A.....	53
Appendix B .....	55
Bibliography.....	58
Vita.....	61

## List of Figures

### Figure

2-1	Optical Absorption.....	4
2-2	Diagram of radiative transitions.....	6
2-3	Donor-to-acceptor pair transition.....	9
2-4	Typical MBE setup .....	13
3-1	Cathodoluminescence setup .....	19
3-2	Photoluminescence setup .....	22
4-1	Determination of optical absorption band gap energies.....	25
4-2	Optical absorption curves of the six samples.....	26
4-3	Cathodoluminescence of GaN .....	28
4-4	Cathodoluminescence of AlGaIn ( $x = 0.10$ ) at constant beam energy .....	30
4-5	Cathodoluminescence of AlGaIn ( $x = 0.10$ ) at constant beam current .....	31
4-6	Cathodoluminescence of AlGaIn ( $x = 0.20$ ) at constant beam energy .....	31
4-7	Cathodoluminescence of AlGaIn ( $x = 0.20$ ) at constant beam current .....	32
4-8	Cathodoluminescence of AlGaIn ( $x = 0.30$ ) at constant beam energy .....	34
4-9	Cathodoluminescence of AlGaIn ( $x = 0.30$ ) at constant beam current .....	35
4-10	PeakFit curve for AlGaIn ( $x = 0.20$ ) .....	36
4-11	PeakFit curve for AlGaIn ( $x = 0.30$ ) .....	36
4-12	Cathodoluminescence of AlN peak ( $x = 0.20$ ) at constant beam current.....	39
4-13	Cathodoluminescence of AlN peak ( $x = 0.20$ ) at constant beam energy .....	40
4-14	Cathodoluminescence of AlN peak ( $x = 0.10$ ) at constant beam current.....	42
4-15	Cathodoluminescence of AlN peak ( $x = 0.10$ ) at constant beam energy .....	42
4-16	CL and PL spectra for the GaN standard.....	44
4-17	CL and PL spectra of AlGaIn ( $x = 0.10$ ).....	45
4-18	CL and PL spectra of AlGaIn ( $x = 0.20$ ).....	45
4-19	CL at constant beam current and PL spectra of AlGaIn ( $x = 0.30$ ).....	47
4-20	CL at constant beam energy and PL spectra of AlGaIn ( $x = 0.30$ ).....	47
B-1	Cathodoluminescence of AlGaIn ( $x = 0.40$ ) at constant beam energy .....	55
B-2	Cathodoluminescence of AlGaIn ( $x = 0.40$ ) at constant beam current .....	56
B-3	Cathodoluminescence of AlGaIn ( $x = 0.50$ ) at constant beam energy .....	56
B-4	Cathodoluminescence of AlGaIn ( $x = 0.50$ ) at constant beam current .....	57



## List of Tables

### Table

3-1	Procedure for Growth of Samples.....	15
4-1	Theoretical and Optical Absorption Experimental Band Gap Energies.....	25
4-2	GaN Transitions Energies .....	28
4-3	Transition Energies for AlGa <sub>N</sub> (x = 0.11 and 0.38) .....	30
4-4	Probable Transition Energies for Al <sub>x</sub> Ga <sub>1-x</sub> N .....	35
4-5	Theoretical and Experimental Band Gap Energies of GaN and AlGa <sub>N</sub> .....	37
4-6	Probable Transition Energies for AlN Buffer Layer .....	41
4-7	Laser Penetration Depths .....	43
4-8	PL Transition Energies for GaN and AlGa <sub>N</sub> samples.....	48
A-1	Periodic Properties of Aluminum, Gallium, and Nitrogen .....	53
A-2	Density of AlN and GaN.....	53
A-3	Electron Penetration Depths for GaN and AlGa <sub>N</sub> .....	54

## Abstract

AlGa<sub>N</sub> and Ga<sub>N</sub> have gained attention in the last few years for their applications in the blue and ultraviolet (UV) wavelength range. However, the majority of the attention has been directed to studying Ga<sub>N</sub> rather than AlGa<sub>N</sub>. AlGa<sub>N</sub> is however of great interest militarily since it has a wide, direct band gap, which makes it suitable for various applications in the military such as plume detection and threat warning systems.

Cathodoluminescence (CL), photoluminescence (PL), and optical absorption were used to characterize AlGa<sub>N</sub> samples grown by molecular beam epitaxy (MBE). These samples utilized an AlN buffer layer to match the AlGa<sub>N</sub> epilayer to the sapphire substrate. CL was run at four different beam energies (2, 5, 10, and 15 keV) with four different beam currents (1, 10, 50, and 90 or 100  $\mu$ A) on a Ga<sub>N</sub> standard, the AlGa<sub>N</sub> samples, and the AlN buffer layer. PL was performed in an attempt to distinguish DAP transitions that were not observed in CL. PL was done on the Ga<sub>N</sub> standard and the AlGa<sub>N</sub> samples ( $x = 0.10, 0.20, \text{ and } 0.30$ ). Optical absorption measurements were performed to get an estimate of the band gap energies for comparison to those obtained in CL and PL. CL and PL were performed at liquid helium temperatures and optical absorption was performed at room temperature. AlGa<sub>N</sub> with different mole fractions of aluminum ( $x = 0.10, 0.20, 0.30, 0.40, \text{ and } 0.50$ ) was studied. Each sample was doped with approximately  $10^{18} \text{ cm}^{-3}$  silicon atoms.

The major finding of this study was that MBE is a good method for growing AlGa<sub>N</sub> with mole fraction of aluminum less than  $x = 0.30$ . Above this mole fraction, either a different growth technique or modifications to the MBE growth cycle are necessary to obtain quality material for semiconductor devices.

## I. Introduction

The III-IV compounds, GaN and AlGa<sub>N</sub>, have garnered attention in the last few years for their applications in the blue and ultraviolet (UV) wavelength range. However, most of the effort has been on studying GaN rather than AlGa<sub>N</sub> and the other ternary and quaternary alloys (8:1). Both GaN and AlGa<sub>N</sub> have wide, direct band gaps, which make them suitable for various applications in the military as well as the civilian sectors. These materials cover a significant spectral range from GaN at 3.4 eV (3646 Å) to AlN at 6.2 eV (1999 Å) making them suitable for military applications (13:1). One such application is in UV detectors that are utilized in plume detection and threat warning systems, which can be outfitted on aircraft, ships, tanks, and other military hardware (6:1). Other applications that could be used in both sectors are light emitting diodes (LEDs), lasers, communication electronics, high-density compact optical-storage-disc systems, short-wavelength optical emitters, and field effect transistors (6:1, 10:44, 14:3841, 15:8505). Furthermore, AlGa<sub>N</sub> and GaN have excellent hardness, high thermal conductivity, high melting points, and good radiation resistance properties that make them attractive for high temperature, high power, and space applications (10:44, 23:1069). These are only some of the applications currently being pursued but as the technology and understanding of these materials increase the uses will escalate.

However, as tempting as these materials seem there are drawbacks. In this study, the quality of AlGa<sub>N</sub> grown on a sapphire substrate was analyzed. A major difficulty in growing AlGa<sub>N</sub> is the inability to find a suitable lattice matched substrate on which to grow it. AlGa<sub>N</sub> and GaN have a significant lateral lattice mismatch with C-plane sapphire, which results in high dislocation densities and stacking faults (4:257, 12:1315, 20:2).

Also, the difference in thermal-expansion coefficients of the epilayer and the sapphire substrate causes compression, which places more strain on the lattice structure (15:8506). Another problem with the sapphire substrate is the fact that it dissociates during the growth process, thus introducing oxygen impurities into the material causing the aluminum to oxidize (20:1). Despite these problems, the sapphire substrate is utilized because of its low cost and wide availability (20:2). An additional disadvantage of AlGa<sub>N</sub> and Ga<sub>N</sub> is the lack of understanding of the native defects, impurity incorporation mechanisms, and their roles during the growth process (20:2). Due to these difficulties, the growth of excellent AlGa<sub>N</sub> and Ga<sub>N</sub> materials is an intricate process. The major growth techniques currently utilized are molecular beam epitaxy (MBE), metal organic vapour phase epitaxy (MOVPE), and metalorganic chemical vapor deposition (MOCVD) (5:1, 10:44).

The objective of this research is to determine the quality of AlGa<sub>N</sub> samples doped with silicon grown by molecular beam epitaxy with mole fractions of aluminum ranging from  $x = 0.10$  to  $x = 0.50$ . The substrate utilized for this study was C-plane sapphire with an AlN buffer layer added between the substrate and the AlGa<sub>N</sub> epilayer. This research employed optical absorption, cathodoluminescence (CL), and photoluminescence (PL) in an attempt to determine the quality of the samples. Optical absorption provided an indication of the band gap energies of the samples. CL and PL were used to characterize the material through the energy levels present. In CL and PL, an electron or a laser beam excites a section of the material causing the production of electron-hole pairs. Material composition and impurities determine the radiative recombinations of these electron-hole pairs. Recombination is dependent on the availability of the energy levels that permit particular transitions, thus, the availability of specific energy levels is a function of the

concentration of the impurity or defect species that is the source of the energy levels (2:2). These two methods will furnish a measurement of the aluminum mole fraction in the AlGa<sub>N</sub> samples. Along with the aluminum concentration, these experiments can provide insight into material uniformity, defects, and impurities in the test samples. Because of the imperfections in the materials such as nonuniformity, defects and impurities, variations in the CL and /or PL data may be observed depending on the location of the electron or laser beam on the sample.

The primary focus of this research was the use of CL to study Ga<sub>N</sub>, AlGa<sub>N</sub> with various mole fractions of aluminum, and the Al<sub>N</sub> buffer in AlGa<sub>N</sub> to determine material quality. The AlGa<sub>N</sub> samples were doped with  $10^{18} \text{ cm}^{-3}$  silicon atoms. CL was performed at beam energies of 2, 5, 10, and 15 keV for Ga<sub>N</sub>, AlGa<sub>N</sub>, and Al<sub>N</sub> buffer layer. Each of the beam energies was run with four different currents, 1, 10, 50, and 90 or 100  $\mu\text{A}$ . The CL and/or PL data represented only one location on each of the samples. Also, the location examined for CL was not the exact location examined in the PL experiment. Not only were the specific spots observed in CL, PL, and optical absorption different but the cross section of the respective beams was also different. In an attempt to differentiate certain transitions, PL was employed. The Ga<sub>N</sub> and three of the AlGa<sub>N</sub> samples (mole fraction of 0.10, 0.20, and 0.30 aluminum) were examined with PL. Optical absorption provided band gap energies for comparison with the energies found in CL and PL.

## II. Theory

The theories presented in the following pages are the basis to understanding the results and conclusions of this research. It is assumed that the reader has basic knowledge of material science and semiconductor band theory. For those either unfamiliar with, or who wish to reexamine some of the basic knowledge of materials and band theory, can refer to the various sources cited in this report. This chapter discusses optical absorption, luminescence, radiative transitions, phonon replicas, laser penetration, electron penetration, and molecular beam epitaxy.

### Optical Absorption

Figure 2-1 best explains optical absorption. An incident light beam strikes the surface of the sample with incident intensity,  $I_i$ . The sample absorbs some of the beam with an intensity,  $I_A$ , part of the beam is transmitted with an intensity,  $I_t$ , another part of the beam is reflected with an intensity,  $I_R$ , and a piece of the beam is scattered at the surface with an intensity,  $I_S$ . Absorption is the ratio of  $I_A$  to the incident light beam,  $I_i$ .

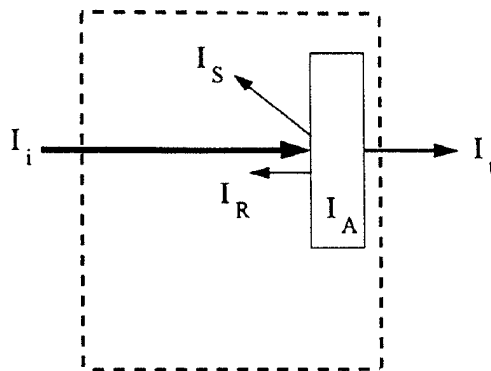


**Figure 2-1.** Optical Absorption (16:4-26).

## Luminescence

When energy is given to a solid, the solid can emit photons in excess of its thermal radiation. This process is termed luminescence. If the excitation source is energetic electrons or cathode rays, then the process is called Cathodoluminescence (CL). On the other hand, if the excitation source is a beam of photons, then the process is called Photoluminescence (22:21). As the excitation source penetrates the sample, the greatest amount of energy is absorbed at or near the surface. This is because of the attenuation of the electrons or photons as they penetrate the test sample. The excitation creates electron-hole pairs. These pairs tend to diffuse away from the excited area in an attempt to restore homogeneity to the structure. The probability of self-absorption in the excited areas is reduced. Hence, luminescence (radiation recombination) escapes from the test sample via the excited surface (2:4). Often in semiconductors, this luminescence is described as electron-hole pair radiative transitions (22:22).

## Radiative Transitions

Since there are numerous energy levels in a crystal, electron and hole recombinations can emit photons with several possible energies. These recombinations can cause multiply lines in the luminescence spectra. The possible radiative transitions are shown in Figure 2-2.

**Process 1**  $\Rightarrow$  Intraband Transition: An electron is excited above the conduction band-edge ( $E_C$ ) and then falls down to the bottom of the conduction band to obtain thermal equilibrium with the lattice. Usually phonon emission occurs with this transition.

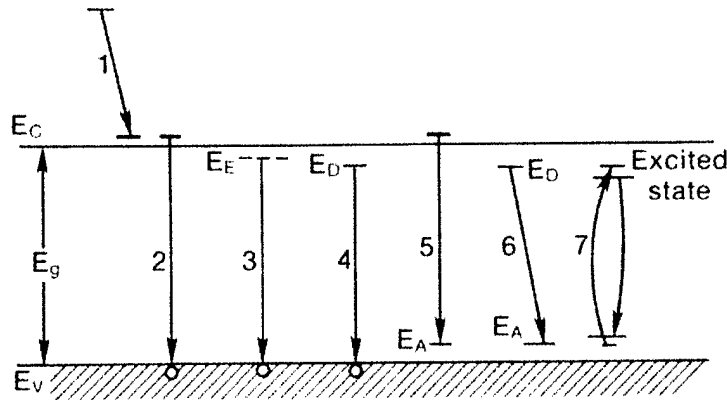


**Figure 2-2.** Diagram of radiative transitions between valence band ( $E_V$ ), conduction band ( $E_C$ ), band gap ( $E_g$ ), and acceptor ( $E_A$ ), donor ( $E_D$ ), and exciton ( $E_E$ ) levels in a semiconductor (22:25).

**Process 2**  $\Rightarrow$  Interband Transition: Direct recombination between a hole in the valence band ( $E_V$ ) and an electron in the conduction band ( $E_C$ ) produces an emission of a photon with energy approximately equal to the band gap energy ( $h\nu \approx E_g$ ). Usually this leads to a broader emission spectrum even though the levels are near the band edge. This broader spectrum is due to the thermal distribution of the carriers. Band-to-band or intraband emission is not a dominant transition because the emitted photons are usually re-absorbed by the crystal (7:15).

**Process 3**  $\Rightarrow$  Exciton Decay at Low Temperatures: An electron-hole pair produced when photons are absorbed is termed an exciton when the electron and hole pair up with each other and the electron orbits the hole. Excitons usually appear as sharp peaks in the absorption edge of direct band gap semiconductors. These transitions can be observed at liquid



helium temperatures because above these temperatures they ionize and come apart. One type of exciton is the free exciton. It occurs when an electron-hole pair moves through the crystal as a pair with a particular kinetic energy. Thus, the luminescence peaks tend to be broader due to the addition of the kinetic energy. The reduced mass of an exciton is less than the effective mass of the electron because the reduced mass of the electron and hole are approximately the same in magnitude. Therefore, the binding energy for a free exciton is smaller than the binding energies of acceptors or donors (7:16). The free exciton recombination energy can be calculated from the equation

$$h\nu = E_g - E_{ex} \quad (1)$$

where  $h\nu$  is the emitted photon energy,  $E_g$  is the band gap energy, and  $E_{ex}$  is the free exciton energy. Besides the free exciton, there is the bound exciton. A bound exciton occurs when a free hole combines with a neutral donor. The hole is bound to the electron in the donor and both orbit the donor ion. The other type of bound exciton occurs when a free electron combines with a neutral acceptor. The bound exciton transition energy can be calculated from the following equation

$$h\nu = E_g - E_{ex} - E_b \quad (2)$$

where  $h\nu$  is the photon energy,  $E_g$  is the band gap energy,  $E_{ex}$  is the free exciton energy, and  $E_b$  is the exciton binding energy. Bound exciton transitions usually produce narrower peaks than the free exciton transition because there is no broadening from kinetic energy ( $KE = 0$ ) (7:16).

**Process 4 & 5  $\Rightarrow$  Impurity Transitions:** These transitions start and/or finish on localized impurity states in the gap. A shallow donor or acceptor level can be extremely close to the conduction and valence band making them hard to distinguish from the band edge. A free-to-bound transition is from the conduction band to an acceptor level or from a donor level to the valence band (22:25). If the transition is direct then the photon energy for the transition is

$$h\nu = E_g - E_i \quad (3)$$

where  $E_g$  is the band gap energy and  $E_i$  is the ionization energy of the acceptor or the donor. A direct or vertical transition occurs when the maximum of the valence band and minimum of the conduction band occur at the same value of the wave vector  $k$ . On the other hand, in an indirect transition the band extrema do not occur at the same wave vector  $k$  (22:23). If the transition is indirect then phonon participation is required to conserve momentum. The photon energy from this transition is shown in the equation

$$h\nu = E_g - E_i - E_p \quad (4)$$

where  $E_g$  is the band gap energy,  $E_i$  is the ionization of the acceptor or the donor, and  $E_p$  is the phonon energy. If the concentration of impurities is high enough, then the impurity levels amalgamate and overlap with the closest intrinsic band. For this reason, it is difficult to distinguish the precise origin of this transition.

**Process 6⇒ Donor-Acceptor Pair Transition:** Donor-acceptor pairs

(DAPs) can produce a series of emission lines (See Figure 2-3). When the electron on a neutral donor recombines with a hole on a neutral acceptor, a photon is produced. The separation distance between the donor and acceptor ion determines the energy of the pair as shown in the equation

$$h\nu = E_g - (E_A + E_D) + e^2/\epsilon r \quad (5)$$

where  $h\nu$  is the donor-acceptor energy,  $E_g$  is the band gap energy,  $E_A$  is the binding energy of the acceptor,  $E_D$  is the binding energy of the donor,  $e$  is charge of the electron,  $\epsilon$  is the dielectric constant, and  $r$  is the separation distance (22:44).

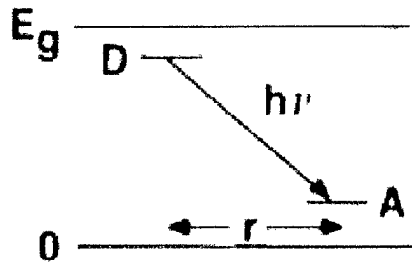


**Figure 2-3.** Donor-to-acceptor pair transition with  $r$  as the separation distance (22:45)

DAPs can be divided into near and far pairs. For the distant or far pairs,  $r$  is large making the last term in the equation (5) small. The combination of near pair and far pair recombinations results in broader unresolved DAP bands. The characteristic shift of the DAP peak is a function of excitation intensity. At higher excitation intensities, the far DAPs will become saturated due to a lower transition probability; hence, the near DAPs then

dominate. Higher excitation intensities cause a greater portion of the near pairs to excite and decay radiatively due to their higher transition probability. As the near DAPs dominate, the intensity of the near pair recombinations increases leading to the shift of the peak to higher energies. A shift of the peak to lower energies can be seen “as the delay after excitation in time-resolved measurements is increased” (22:35). This characteristic feature of DAPs distinguishes them from other recombination transitions. DAPs can occur near the band edge. In PL, DAPs are observed as numerous sharp lines providing a means of differentiating them from other PL transitions (22:45). However, to observe these numerous sharp lines, the PL experiment must provide extremely high resolution. For normal spectrometer resolutions the DA pair peak is a broad unresolved peak.

### Phonon Replicas

A series of lines or peaks separated by a phonon energy of  $\hbar\omega$  are called phonon replicas. They are usually associated with a sharp emission line and occur at lower energies than the sharp peak (22:42, 7:67). The equation for the energy of the phonon replicas is represented in the equation

$$h\nu = E_g - E_s - n \hbar\omega \quad (6)$$

where  $h\nu$  is the photon energy,  $E_g$  is the band gap energy,  $E_s$  is the energy of the recombination level,  $n$  is the number of phonons, and  $\hbar\omega$  is the phonon energy (22:43). Each successive phonon replica decreases in intensity compared to the previous phonon

replica. Also, the probability of additional phonon replicas is reduced with each consecutive phonon replica.

### Laser Penetration

The excitation source used for photoluminescence is the laser. As the laser penetrates deeper into the sample, it excites different regions of the sample. It is thus important to know how far the beam penetrates into the sample to understand the recombination mechanics occurring in the surface. Beer's law supplies insight into laser penetration through the equation

$$I(x) = I(0)e^{-\alpha x} \quad (7)$$

where  $I(x)$  is the intensity of the light as a function of the beam penetration  $\{I(x)$  is equal to the intensity at depth  $x\}$ ,  $I(0)$  is the intensity at  $x = 0$ ,  $\alpha$  is the absorption coefficient of the material at a particular wavelength, and  $x$  is the depth of the beam penetration (22:28). Absorption is greatest at the surface because of the exponential attenuation of the laser beam as it penetrates the sample.

### Electron Penetration

The excitation source for cathodoluminescence is an electron beam. It is of particular importance to know in which material layers electron excitation is occurring and thus where the transitions are taking place. Since different beam energies were used in this research, the determination of electron beam penetration at these different energies is essential. The samples in this research have an AlN buffer layer between the sapphire substrate and the AlGaIn epilayer. A GaN epilayer grown on a sapphire substrate was utilized as a standard in this research. The following paragraph presents a simplified version of this complex process of electron beam penetration.

When a beam of electrons penetrates a solid, they are scattered either elastically or inelastically. “Electronic stopping is due to inelastic collisions with atomic electrons in which the incident electron excites or ejects atomic electrons with loss of energy” (9:43). Because the electron is a light particle, the momentum transfer is diminutive but the energy loss is big. Nuclear stopping is an elastic collision between the electrons and the atomic nuclei. A transfer of energy and momentum occurs in nuclear stopping. For simplicity, it was assumed that the electrons are mostly colliding with other electrons in the lattice; therefore, only electron-electron interactions are considered (2:17). The maximum depth of the electron beam penetration into the structure can be determined by Kanaya-Okayama equation

$$R = [0.0276A/(Z^{0.89}\rho)]E_0^{1.67} \quad (8)$$

where R is the maximum depth in  $\mu\text{m}$ , A is the atomic weight in  $\text{gmole}^{-1}$ , Z is the atomic number,  $\rho$  is the density in  $\text{gcm}^{-3}$ , and  $E_0$  is the incident beam energy in keV (22:58).

### Molecular Beam Epitaxy

“Molecular beam epitaxy (MBE) is an epitaxial process involving the reaction of one or more thermal beams of atoms or molecules with a crystalline surface under ultrahigh vacuum conditions ( $\sim 10^{-10}$  Torr)” (18:333). This growth technique is capable of obtaining precise control over chemical composition and doping profile. “Single-crystal multilayer structures with dimensions of the order of atomic layers can be made using MBE” (18:333). Separate effusion ovens or cells provide elements such as gallium, aluminum, and dopants for epilayer growth. Figure 2-4 shows a typical MBE growth system. The temperature of the cells can be adjusted to the appropriate evaporation rate. Shutters at the end of each cell are the on/off switch for the cells. The main shutter is an

additional safeguard to prevent any leakage of the cells when they are not in use. The sample exchange load lock and gate valve allows the substrate to be changed while maintaining the vacuum. The substrate is heated to the appropriate temperature for growth and rotated continuously to produce uniform epitaxial layers (18:336). Typical substrate temperatures range from 400 to 900°C (18:338). Normal growth rates vary from 0.001 to 0.30  $\mu\text{m}/\text{min}$  (18:338).

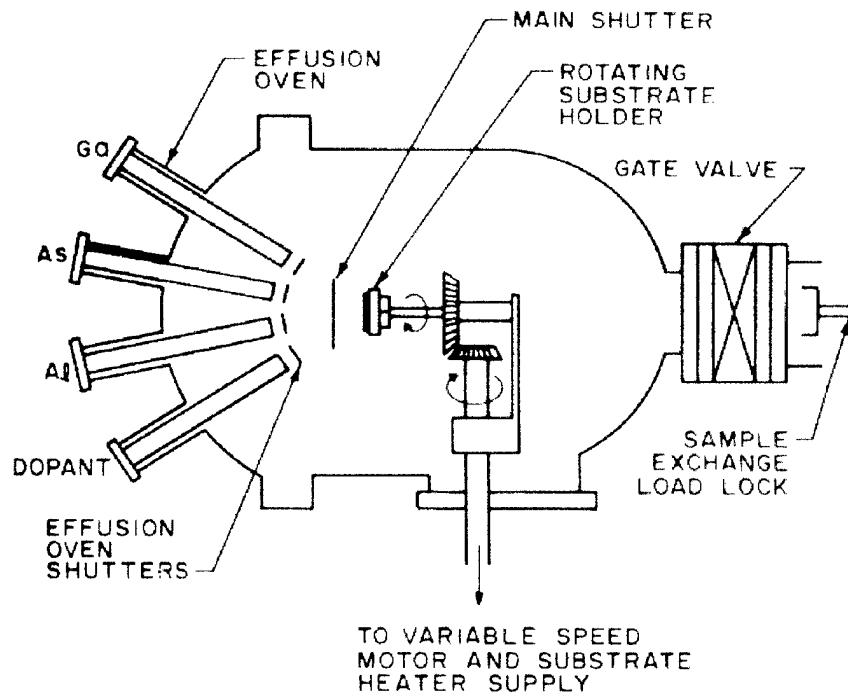


**Figure 2-4.** Typical MBE setup

The low temperature and low growth rate of the MBE process can produce several unique alloy compositions and doping profiles. Because of the low temperature and growth rate, doping profile can be accurately controlled and various dopants can be utilized in MBE as compared to other techniques such as vapor phase epitaxy (VPE). An

example of a unique structure grown by MBE, is the superlattice. A superlattice is a periodic structure made up of alternating ultra thin layers with a period smaller than the electron free path (18:338).



### III. Methodology

The procedures and equipment utilized to obtain the optical absorption, CL, and PL data are explained in this section. Any conditions that limit the experiment will be examined in this section. This chapter will cover sample information, molecular beam epitaxy, sample mounting and preparation, optical absorption system setup, cathodoluminescence system setup, and photoluminescence system setup.

#### Sample Information

The AlGaN samples were grown on a sapphire ( $\text{Al}_2\text{O}_3$ ) substrate oriented in the 0001 direction (c-plane) using molecular beam epitaxy. The samples are approximately 1  $\mu\text{m}$  thick. Prior to growth, the back of the substrate was metallized with 2500 Å of Titanium and 2500 Å Platinum. Then the front of the substrate was etched with  $\text{H}_2\text{SO}_4$  and  $\text{H}_3\text{PO}_4$  in a 3:1 ( $\text{H}_2\text{SO}_4:\text{H}_3\text{PO}_4$ ) ratio for 10 minutes at  $200^\circ\text{C}$ . Deionized water was used to rinse the wafers and liquid nitrogen boil off was used to dry the samples. The molecular beam epitaxy growth schedule for the samples are shown in Table 3-1. The test samples were doped with  $10^{18} \text{ cm}^{-3}$  silicon atoms.

**TABLE 3-1**

Procedure for Growth of Samples

Material	Dopant	Time (seconds)	Thickness (Å)	Temperature (°C)
$\text{NH}_3$		600		1016
$\text{NH}_3$		300		
AlN		300	200	871
$\text{NH}_3$		180		
AlGaN	Si	3600	10000	

## Molecular Beam Epitaxy

A modified Varian 360 molecular beam epitaxy system utilizing ammonia as a nitrogen source was used to grow the samples for these experiments. The AlGa<sub>N</sub> samples were doped with silicon. The growth temperature for the III-nitride films was 800°C with the chamber background pressure at about  $8 \times 10^{-9}$  Torr. The temperature of the samples was monitored by an optical pyrometer, which operated in the 0.9-1.1  $\mu\text{m}$  range. An emissivity setting of  $\epsilon = 0.4$  was used because of the assumption that sapphire was transparent at this wavelength. Standard Knudsen cells supplied the elemental aluminum, gallium, and silicon for epilayer growth. The cell rates were 0.5  $\mu\text{m/hr}$ . A cracking gas injector equipped with a pyrolytic boron nitride diffuser plate provided the ammonia during growth. "The gas cracker was operated at  $\sim 50^\circ\text{C}$  to prevent condensation of the adiabatically expanding ammonia on the cracker walls." (21:3121). A corrosive service mass flow controller provided ammonia at the specified rate. This rate corresponded to a "line-of-sight beam equivalent pressure of  $8.2 \times 10^{-6}$  Torr" (21:3121).

## Sample Preparation and Mounting

For CL and PL, the samples were cut to approximately 3 mm by 3 mm dimensions. Prior to mounting, the samples were cleaned with TCE, acetone, and methanol. The Ga<sub>N</sub> standard,  $\text{Al}_{0.10}\text{Ga}_{0.90}\text{N}$ ,  $\text{Al}_{0.20}\text{Ga}_{0.80}\text{N}$ ,  $\text{Al}_{0.30}\text{Ga}_{0.70}\text{N}$ ,  $\text{Al}_{0.40}\text{Ga}_{0.60}\text{N}$ , and  $\text{Al}_{0.50}\text{Ga}_{0.50}\text{N}$  were examined using CL. For CL, after cleaning, indium solder was added to the samples to improve the contact so as to allow surface charge due to the electron beam to dissipate. A bead of rubber cement was used to attach the samples for CL to the copper sample holder. In addition to the solder, a copper plate in contact with the indium solder aided in

the dissipation of the electric charge build-up. For PL, the samples were mounted with rubber cement to the copper sample holder. The four samples used in PL were GaN,  $\text{Al}_{0.10}\text{Ga}_{0.90}\text{N}$ ,  $\text{Al}_{0.20}\text{Ga}_{0.80}\text{N}$ , and  $\text{Al}_{0.30}\text{Ga}_{0.70}\text{N}$ .

#### Optical Absorption System Setup

For optical absorption, a Lambda 19 spectrometer capable of ultraviolet and visible wavelength ranges was utilized. The Lambda 19 is a self-calibrating instrument which has a scan range of 180 nm to 900 nm. The spectrometer has two radiation sources, a deuterium lamp (DL) and a halogen lamp (HL). The deuterium lamp was used for the UV measurements, leaving the halogen lamp for the visible and near infrared measurements. A photomultiplier tube (PMT) was the internal detector of this system. All absorption data was taken at room temperature.

#### Cathodoluminescence System Setup

The CL setup is shown in Figure 3-1. In this system, the helitran fits into top of the vacuum chamber. Due to the thickness of the helitran's sample holder, the samples are slightly displaced from the center of the chamber, which is the optimal position for excitation by the electron beam. The electron beam can be steered by deflection plates but if the beam gets too close to these plates, they can cut off some of the beam or cause beam distortion. This was not a limitation unless the samples were offset from the optimal placement as in this experimental setup. The off-center position of the sample thus limited the useful beam energies to no higher than 15 keV and no lower than 2 keV. However, some of the data at 15 keV with high beam currents showed electron beam distortion. Also, this reduced the number of samples that could be usefully included on the sample holder from about four to two, i.e. the limited electron beam deflection reduced the

number of samples to two, one sample mounted on the front of the holder and the other on the back. A calibrated silicon diode was mounted approximately one centimeter from the sample on the front side of the sample holder to monitor temperature. The temperature of the samples was approximately 10 K.

A helitran dewar was used to transfer liquid helium to the cold finger (sample holder). A turbomolecular pump with a mechanical pump provided the vacuum of about  $10^{-7}$  Torr. Pump down time was dependent upon how long the chamber was at atmosphere. Typical pump down time ranged from about 1 to 3 hours. Two devices were utilized to monitor the vacuum, a thermocouple vacuum gauge and an ionization gauge. An electron gun was the excitation source, which caused the luminescence of the sample. Optics were used to collect and focus this luminescence into the grating spectrometer. The light or luminescence was then detected by a liquid nitrogen cooled photomultiplier tube (PMT) and output to a computer. The PMT has an almost constant reponsivity over a wavelength range of 150 nm to 850 nm. Operation temperature for the PMT was  $-40^{\circ}\text{C}$ .

For CL, the spectrometer is calibrated using a mercury lamp. The slits of the spectrometer were set to 10  $\mu\text{m}$ . Three standard spectral lines of mercury in the range of the data that was taken were 3125.7, 3131.7, and 3341.5  $\text{\AA}$ . Then the spectrometer was run over a range that would encompass the standard spectral lines. After the experimental spectral line was found, it was compared to the standard. The difference was then used to correct the acquired data as appropriate. Due to the swings in climate control, the system was calibrated each day that data was collected. The calibration correction was between +7.20 to +9.00  $\text{\AA}$  for the CL data.

The CL excitation source is a Kimball Physics EMG-12 Electron Gun and EGPS-12 power supply with enhanced beam current option that allows its use in vacuum physics and surface physics applications. This gun has a beam energy adjustment from 100 eV to 20 keV as well as a beam current adjustment of 10 nA to 100  $\mu$ A. The spot size of the beam on the sample ranges from 1.0 mm to 25 mm with the enhanced beam option. The beam diameter utilized for this experiment was approximately 1 to 3 mm on the sample.

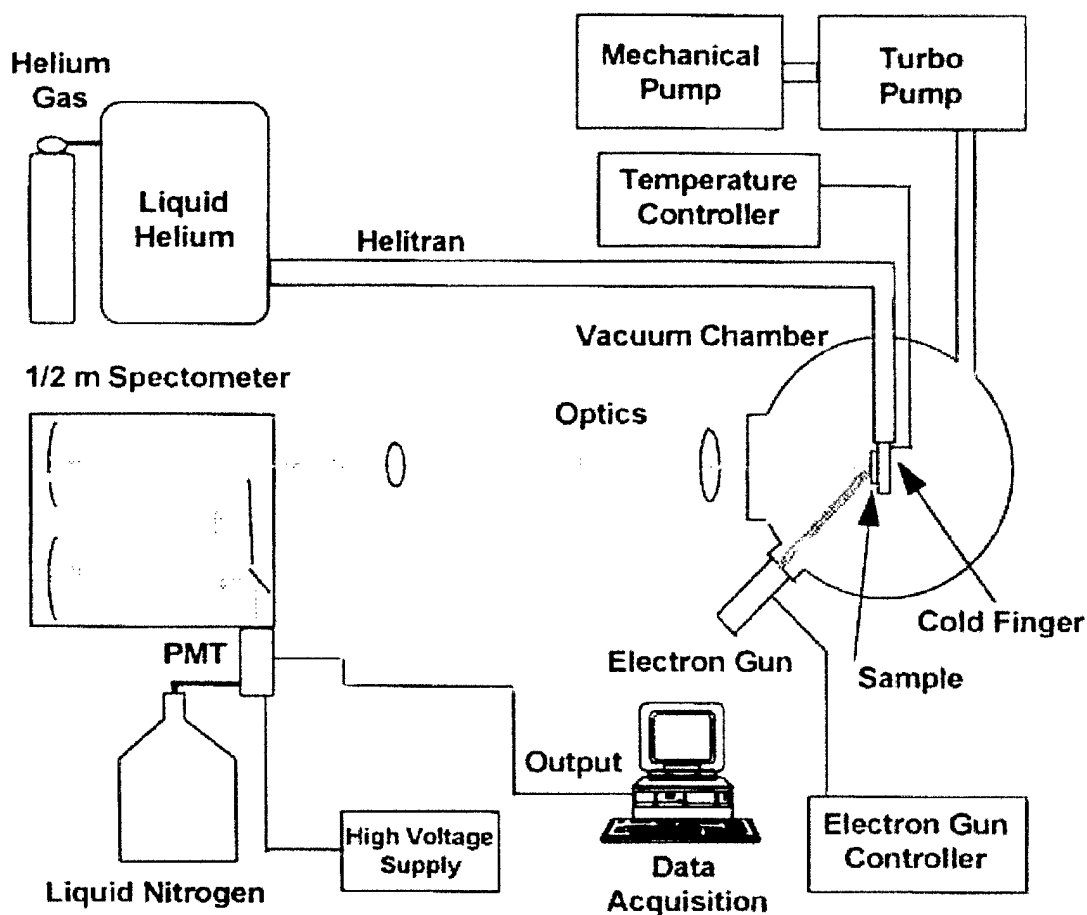


**Figure 3-1.** Cathodoluminescence setup for low temperature experimentation (16:4-17).

### Photoluminescence System Setup

The PL setup, shown in Figure 3-2, is similar to the CL setup. The cold finger, which can support 16 samples, was inserted in the Janis 10DT liquid helium variable temperature cryostat. The cryostat is composed of a liquid helium reservoir that maintains a temperature of about 2 K to 300 K. A liquid helium level meter monitored the amount of helium in the reservoir. A reservoir of liquid nitrogen at approximately 77 K insulated the liquid helium from the environment. A vacuum jacket isolated the two reservoirs from each other and acted as an insulator for the liquid nitrogen. A turbomolecular pump backed by a mechanical pump was utilized to bring the vacuum jacket from atmospheric pressure (760 Torr) to  $10^{-6}$  Torr. A needle valve regulated the flow of the liquid helium to the sample chamber. The sample temperature was maintained at approximately 10 K. A temperature controller accompanied by a silicon temperature probe monitored the temperature of the samples. An argon ion laser provided the excitation source that caused the sample to luminesce. This luminescence from the sample was focused and collected by optics into the spectrometer as in the CL setup. It was then detected by a liquid nitrogen cooled photomultiplier tube (PMT) and output to a computer, as in the CL setup. The spectrometer calibration for the PL system was the same as that of the CL system. A long pass filter was placed in front of the slit to filter out undesired spectral lines from the argon laser.

For PL, a UV laser with a higher energy than the band gap energy of the material must be used. This is necessary to excite the electrons of the material from the valence band to the conduction band of the material. If the energy were lower, then no electrons would be excited to the conduction band. In this study, an argon laser was the excitation

source. The argon laser used was a Spectra Physics 2085 capable of generating up to 2 Watts ultraviolet laser output. It was operated at 275.4 nm (4.502 eV), which is above the band gap of the samples studied.

Finally, there were some limiting factors concerning the power of the PL laser setup. The laser wavelength of 275.4 nm (deep UV) needs beam steering optics to position the laser light onto the sample due to the orientation of the argon laser. Unfortunately, the best optics were not available for this test. As a result, optics that had a lower transmission in the UV, were used to steer the laser beam. This resulted in the 2 Watt laser output (measured in front of the laser head) to be reduced to a 200 milli-watt beam (power on the test specimen).

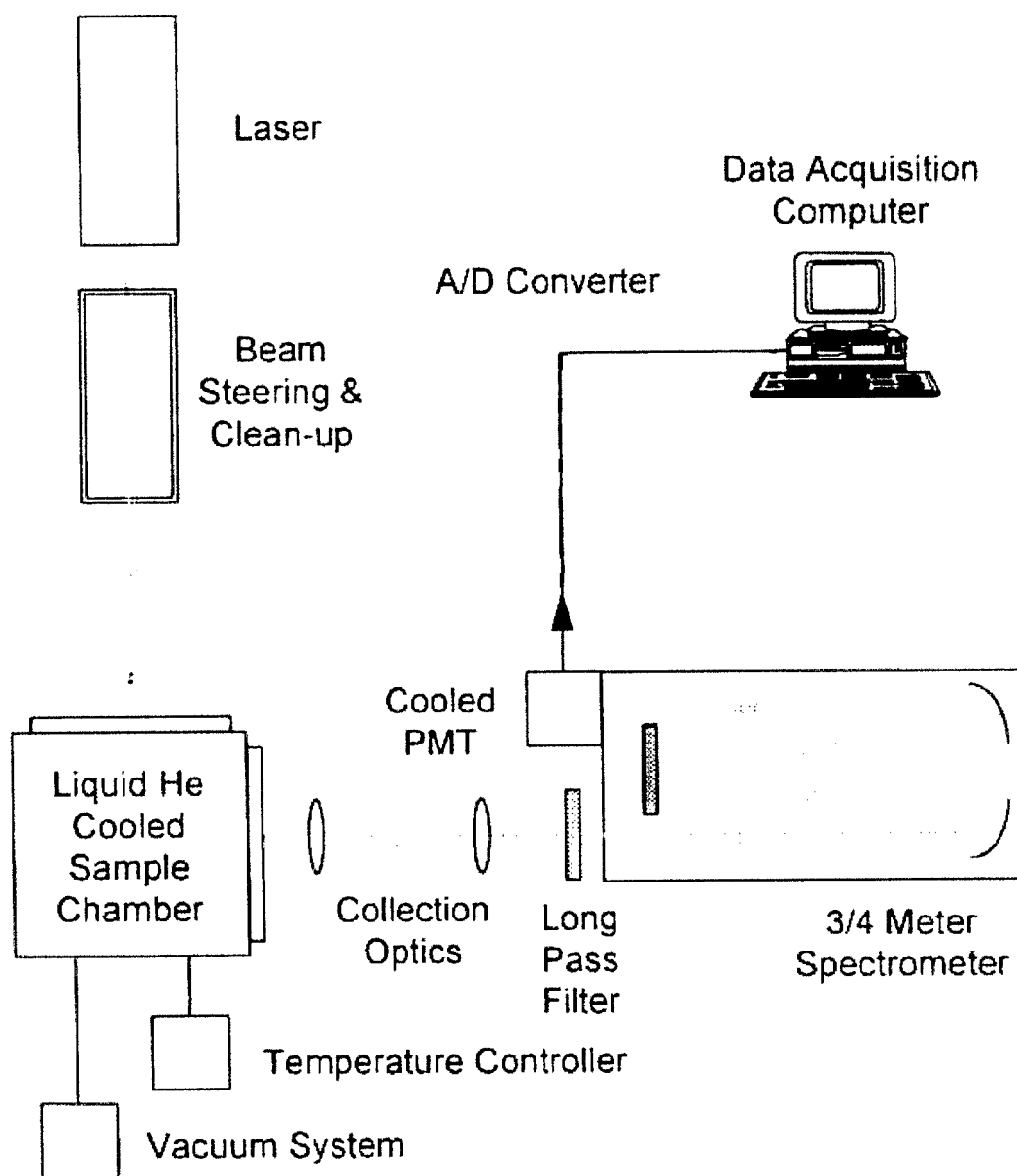


**Figure 3-2.** Photoluminescence setup for low temperature experimentation (16:4-2).



#### IV. Results and Discussion

As stated in the introduction, the focus of this research is  $\text{Al}_x\text{Ga}_{1-x}\text{N}$  doped with silicon. GaN was studied for use as a standard for comparison. Five samples were grown by MBE with mole fractions of aluminum (nominally  $x = 0.10, 0.20, 0.30, 0.40$ , and  $0.50$ ) and were doped with  $10^{18} \text{ cm}^{-3}$  silicon atoms. Optical absorption was performed on these samples as well as the GaN standard. Absorption data provided an estimate of band gap energies to compare with those energies found in CL and PL. For the CL experiment, four different beam energies (2, 5, 10, and 15 keV) were utilized with four different beam currents (1, 10, 50, and 90 or 100  $\mu\text{A}$ ). Not only were the band edge energies of the AlGa $\text{N}$  studied but also the AlN peaks from the buffer layer were run with the four energies at the four currents. PL was performed to try to distinguish DAPs from other radiative transitions.

The positions of the peaks for CL and PL were determined with the aid of a program called PeakFit. PeakFit is a non-linear curve-fitting software developed by Jandel Scientific. From the spectra, the number of peaks was approximated. Arbitrary peaks were selected and gaussian amplitude was used as the appropriate non-linear curve to fit each of the spectrum (see Figures 4-10 and 4-11 on pages 36).

##### Optical Absorption

Optical absorption band gap energies for the materials studied are listed in Table 4-1. The experimental values of the absorption edge were obtained by curve fitting the absorption data for each of the samples (see Figure 4-1). The oscillatory behavior or the “ringing” seen in the data of Figure 4-1 is due to the light being reflected multiply times between the parallel surfaces of the sample. To prevent this ringing, the sample

surfaces must not be parallel but wedged, which was not the case in this study. The band gap was determined to be the point where the slope of the curve intersects the level off line. The slope of the data is denoted as (b). The level off line is where the data is no longer descending but has leveled off. This is the average of the oscillations and is denoted by the line labeled (a). The band gap energies were all determined by this method. Figure 4-2 shows the absorption curves for all six samples. The arrows dropping from the curves indicate the band gap energies as listed in Table 4-1. Theoretical band gap energies at room temperature and assuming a linear function were calculated using the equation

$$E_g(x) = xE_{g\text{AlN}} + (1-x)E_{g\text{GaN}} \quad (9)$$

where  $E_g(x)$  is the band energy as a function of aluminum mole fraction,  $E_{g\text{AlN}}$  is the band gap energy of AlN (6.2 eV),  $E_{g\text{GaN}}$  is the band gap energy of GaN (3.4 eV), and  $x$  is the mole fraction of aluminum (12:1378, 13:1). As seen in Table 4-1, the experimental band gap of the GaN standard is close to the theoretical band gap. The band energies should increase in energy as the aluminum concentration increases. However, the  $x = 0.40$  sample shows a slight decrease in the band gap energy as compared to the  $x = 0.30$  sample. Also, the theoretical values of the aluminum mole fraction of the samples investigated differ from the experimental values. This is probably because the mole fraction of aluminum does not match the grower's specified mole fraction. Other possibilities for data fluctuation are structural disorder, point defects, or impurities such as oxygen and silicon creating shallow defects (5:2).

From the optical absorption data and equation (9), the AlGaIn ( $x = 0.10, 0.20$ , and  $0.30$ ) mole fractions are more likely  $x = 0.04, 0.10$ , and  $0.13$  mole fraction of aluminum.

The AlGa<sub>N</sub> (x = 0.40 and 0.50) have an aluminum concentration more appropriate to 0.12 and 0.17, respectively. Note all absorption data was taken at room temperature.

**TABLE 4-1**

Theoretical and Optical Absorption Experimental Band Gap Energies

Material	Experimental Band Gap Energy at Room Temperature	Theoretical Band Gap Energy at Room Temperature
GaN	3.410 eV (3635 Å)	3.40 eV (3646 Å)
Al <sub>0.1</sub> Ga <sub>0.9</sub> N	3.514 eV (3528 Å)	3.68 eV (3369 Å)
Al <sub>0.2</sub> Ga <sub>0.8</sub> N	3.689 eV (3360 Å)	3.96 eV (3130 Å)
Al <sub>0.3</sub> Ga <sub>0.7</sub> N	3.786 eV (3274 Å)	4.24 eV (2924 Å)
Al <sub>0.4</sub> Ga <sub>0.6</sub> N	3.750 eV (3306 Å)	4.52 eV (2742 Å)
Al <sub>0.5</sub> Ga <sub>0.5</sub> N	3.893 eV (3184 Å)	4.80 eV (2582 Å)

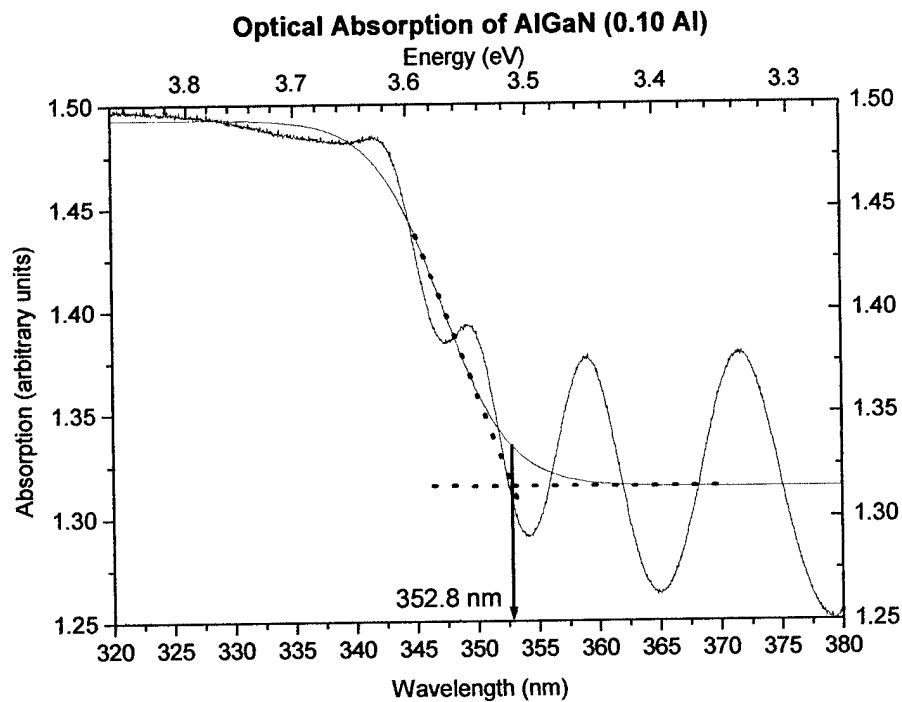


**Figure 4-1.** Determination of optical absorption band gap energies for GaN & AlGa<sub>N</sub>

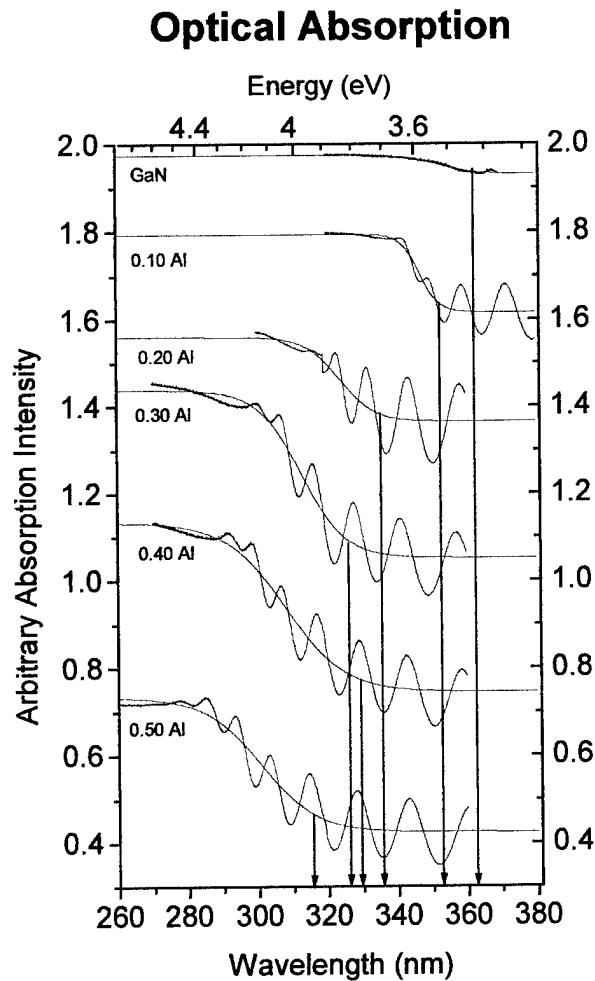


**Figure 4-2.** Optical absorption curves for GaN and AlGaIn samples

### Cathodoluminescence

The key points one looks for in CL as well as PL were the shape and position of the peak or peaks in the spectra. The aluminum concentration can be estimated by determining the exciton peak's wavelength or energy. Usually, the exciton peak is the highest energy peak but not necessarily the highest intensity peak in the spectrum. Other peaks that can be observed in CL and PL data are DAPs and other radiative transitions. The DAPs and these other transitions are indicators of impurities and defects in the

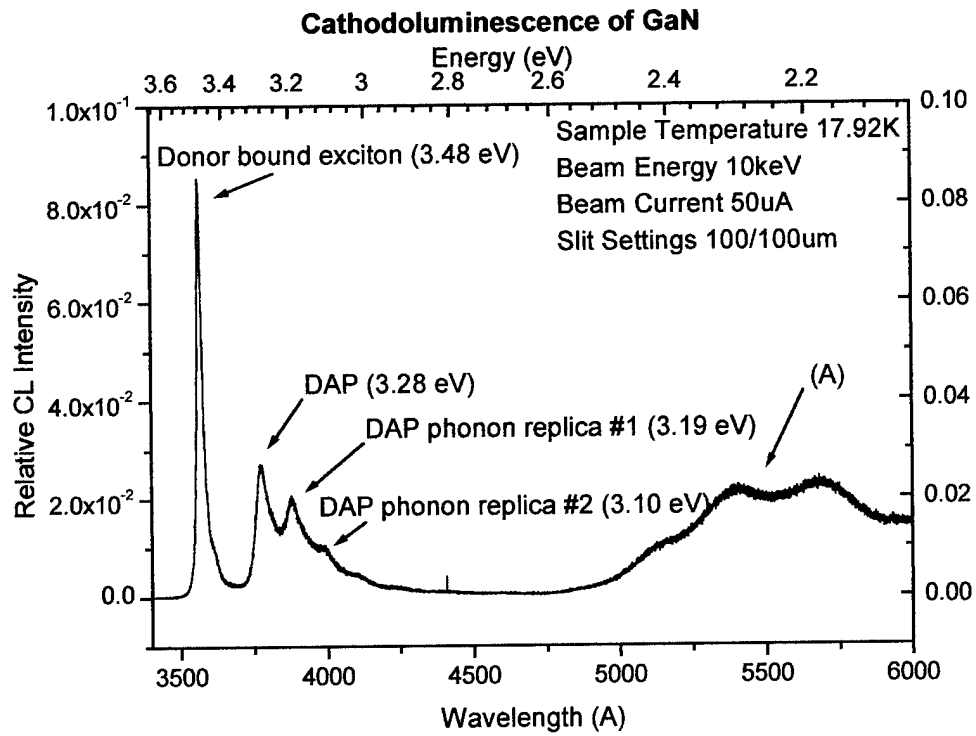
material. To carry out such an analysis, it was important to know in which layer these transitions were occurring. Therefore, it was paramount to determine electron beam depth penetration. The electron beam penetration depths for the different samples are listed in Appendix A. All beam penetration depths were within the AlGaIn epilayer except for a beam energy of 15 keV, which penetrated into the sapphire substrate. With the analysis of the exciton peak, DAP peaks, and electron beam penetration depth, an evaluation of material quality can be achieved. It was these three topics that were the focus in the assessment of the CL data.

#### GaN Standard

The GaN standard is the first to be scrutinized. This will provide the foundation for the discussion of the AlGaIn samples. Table 4-2 lists transition energies reported in the literature compared with those found in this CL study. From the cathodoluminescence spectrum (Figure 4-3), a donor bound exciton, a DAP, and two phonon replicas were identified. The energies of the transitions correlated well with values found in the literature (see Table 4-2). The overall width of the spectra is 250 Å (0.249 eV). The peaks labeled (A) are termed “yellow emission” which is believed to be from a complex of intrinsic defects and oxygen (33:13, 14:51). The “yellow emission” dominated the spectra for the 1 µA runs at 2, 5, 10, and 15 keV. However, at higher currents and different beam energies, the “yellow emission” was approximately the same intensity as the DAP and phonon peaks (see Figure 4-3). There was no characteristic shift of the DAP peak observed in the CL data. Therefore, PL was performed to see if the shift could be observed.

**TABLE 4-2****GaN Transition Energies**

GaN Radiative Transitions	Values obtained from the Literature	Experimental Transition Energy
Neutral donor bound exciton	3.4758 eV (20:8)	3.48 eV
DAP	3.285 eV (5:2)	3.28 eV
DAP phonon replicas	-----	3.19 eV and 3.10 eV

**Figure 4-3. Cathodoluminescence of GaN**

### AlGaN Samples

Utilizing the GaN as a basis, AlGaN was studied. An examination of AlGaN ( $x = 0.10$ ) shows a material that has a relatively sharp, narrow spectrum when compared to the other samples. The spectrum had a width of 200 Å (0.202 eV). Figures 4-4 and 4-5 shows the peak at different beam currents and energies, respectively. As seen, there are minute changes in peak position as the electron beam penetrates further into the sample or the intensity is increased. As stated earlier, the position of the peak does not correlate with a mole fraction of aluminum of  $x = 0.10$ . This sample has a shoulder (B) on the lower energy side of the sharp peak. This shoulder has not been identified at this time. The sharp spectrum itself is actually composed of two peaks, believed to be a bound exciton, and a DAP. These peaks were identified by spectral decomposition using the program PeakFit and compared with reported values from the literature. Tables 4-3 and 4-4 (page 35 for Table 4-4) compare values found in the literature with the CL values obtained in this study. DAPs could not be conclusively distinguished from the other transitions, since there was no characteristic shift with increased intensity or beam current. Also, there were no “yellow emission” peaks around 5430 Å as in the GaN sample (20:50).

The AlGaN with  $x = 0.20$  was examined as seen in Figures 4-6 and 4-7. Compared to  $x = 0.10$ , this peak was wider with a width of 350 Å (0.340 eV). This supports the assumption that as the aluminum mole fraction increases, the oxygen introduced by the nitrogen source or dissociation of the sapphire wafer, forms aluminum oxide (29:3123, 33:13). This impurity as well as others

contributes to the broadening of the spectrum. As in the previous sample ( $x = 0.10$ ), the mole fraction of aluminum is in question and no “yellow emission” or DAP peak shift was observed.

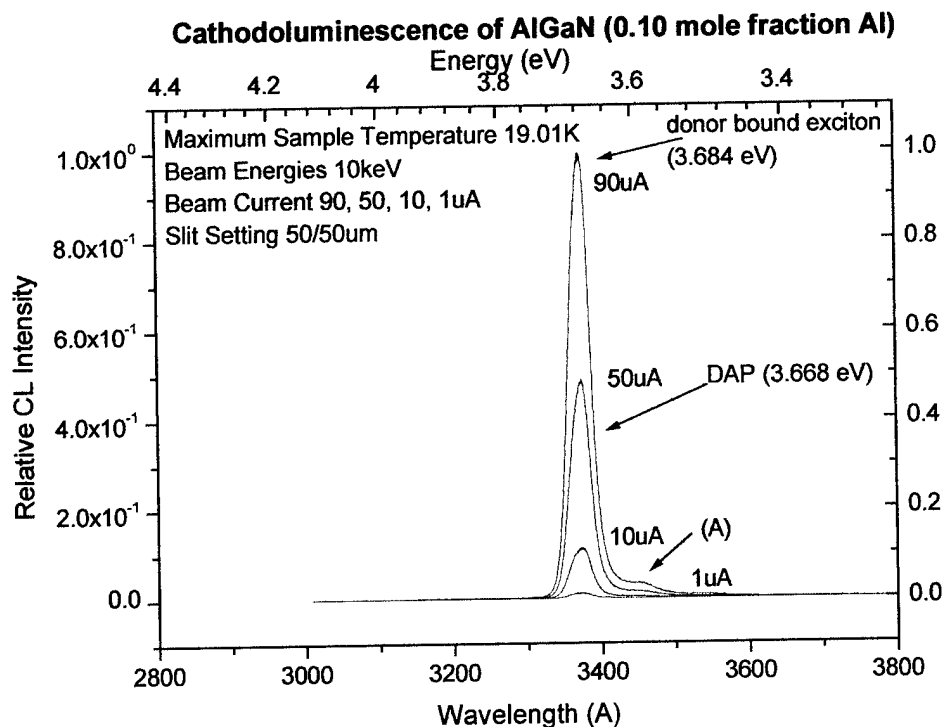


**Figure 4-4.** Cathodoluminescence of AlGa<sub>N</sub> ( $x = 0.10$ ) at constant beam energy

**TABLE 4-3**

Transition Energies for AlGa<sub>N</sub> ( $x = 0.11$  and  $0.38$ )

Transitions	Al <sub>0.11</sub> Ga <sub>0.89</sub> N	Al <sub>0.38</sub> Ga <sub>0.62</sub> N
Donor bound exciton	3.735 eV (3319 Å)	4.198 eV (2953 Å)
DAP #1	3.623 eV (3422 Å)	4.105 eV (3020 Å)
DAP #2	N/A	3.892 eV (3185 Å)

The values in this table were obtained from reference 21 page 3122.



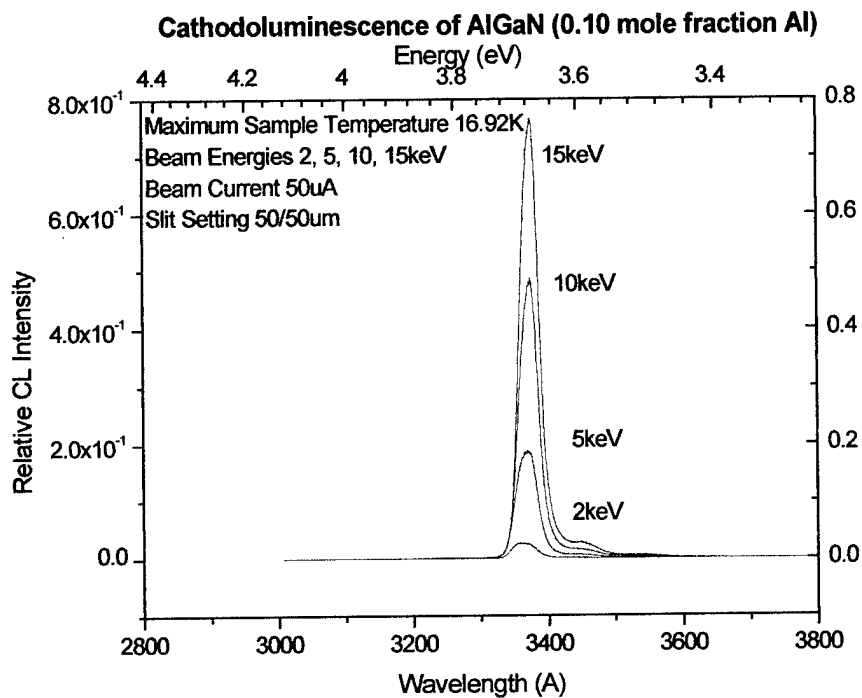


**Figure 4-5.** Cathodoluminescence of AlGa<sub>N</sub> ( $x = 0.10$ ) at constant beam current

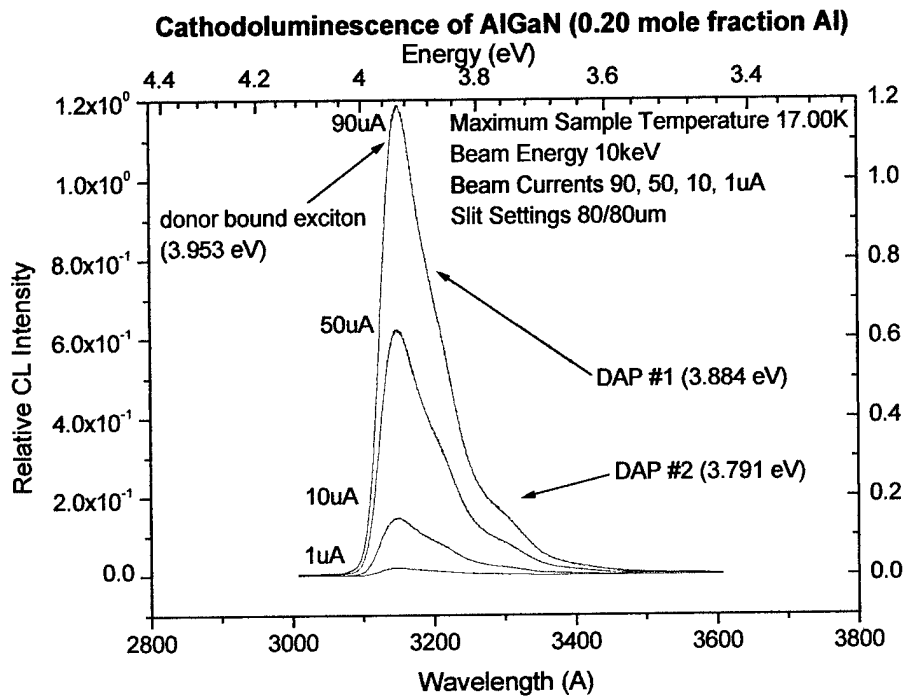


**Figure 4-6.** Cathodoluminescence of AlGa<sub>N</sub> ( $x = 0.20$ ) at constant beam energy

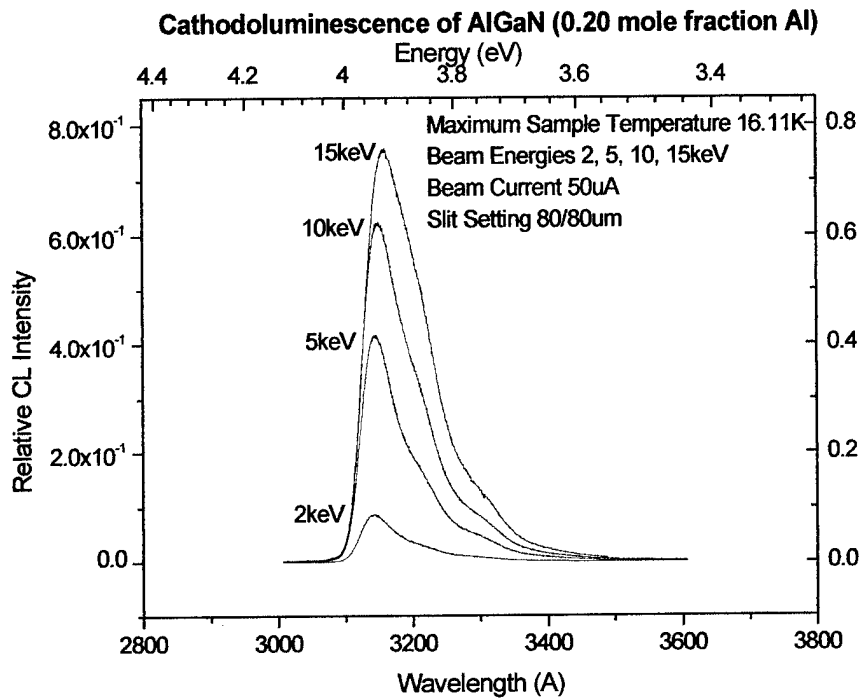


**Figure 4-7.** Cathodoluminescence of AlGa<sub>N</sub> ( $x = 0.20$ ) at constant beam current

The most interesting spectra occurred from the sample with a mole fraction of  $x = 0.30$  aluminum. The width of the peak was  $700 \text{ Å}$  ( $0.622 \text{ eV}$ ) possibly indicating an increase in the impurities and defects in the material. The bound exciton and two DAPs were identified and compared to the literature (see Tables 4-3 and 4-4). Figures 4-8 and 4-9 show the spectra at a constant beam energy and constant beam current. As the beam energy increases the dominant peak (highest intensity) changes from the bound exciton to the second DAP. The first DAP is probably associated with the silicon dopant (21:3123). The second DAP has not been conclusively determined but it is believed to be associated with an extrinsic oxygen impurity (21:3123). The most probable reason for the shifting of the dominant peaks is an increase in the concentration of oxygen as the sample

penetration increases (see Appendix A for electron penetration depths). The oxygen from the ammonia source and/or the dissociation of the sapphire wafer will be localized more heavily near and in the AlN buffer layer. The concentration of oxygen increases as the beam penetration depth increases, resulting in the growth of this shallow donor peak (DAP#2) (see Figure 4-8). There is some controversy over the extrinsic oxygen impurity. The silicon doping of  $\sim 10^{20} \text{ cm}^{-3}$  can suppress the diffusion of the oxygen from the sapphire wafer, therefore, the oxygen impurity from the dissociation of the wafer should be negligible for the samples studied, which were doped with  $\sim 10^{18} \text{ cm}^{-3}$  silicon atoms. However, the reference cited makes no statement of silicon doping suppressing the diffusion of oxygen from the ammonia source (20:1). Therefore, the assumption that the third peak is the shallow donor associated with oxygen could be valid. Note that assignment of DAP peaks was accomplished by comparing values obtained in this study to those in the literature. There was no characteristic shift of the DAP peaks observed in this CL data and no “yellow emission” was observed.

The measured band gap energies of the AlGaN ( $x = 0.40$  and  $0.50$ ) do not match the theoretical values for the mole fraction specified (see Tables 4-4 and 4-5 on pages 35 and 37). These two samples had spectra with widths of  $500 \text{ \AA}$  ( $0.467 \text{ eV}$ ) and  $800 \text{ \AA}$  ( $0.694 \text{ eV}$ ), respectively. At different beam currents and energies, there were slight peak shifts in the spectra. Thus, no DAP peak shifts were observed in any of the CL data and no “yellow emission” was detected. These samples were not examined in detail since they did not provide any new

information over and above that obtained from the other samples examined in this research. However, the plots for these samples are included in Appendix B.

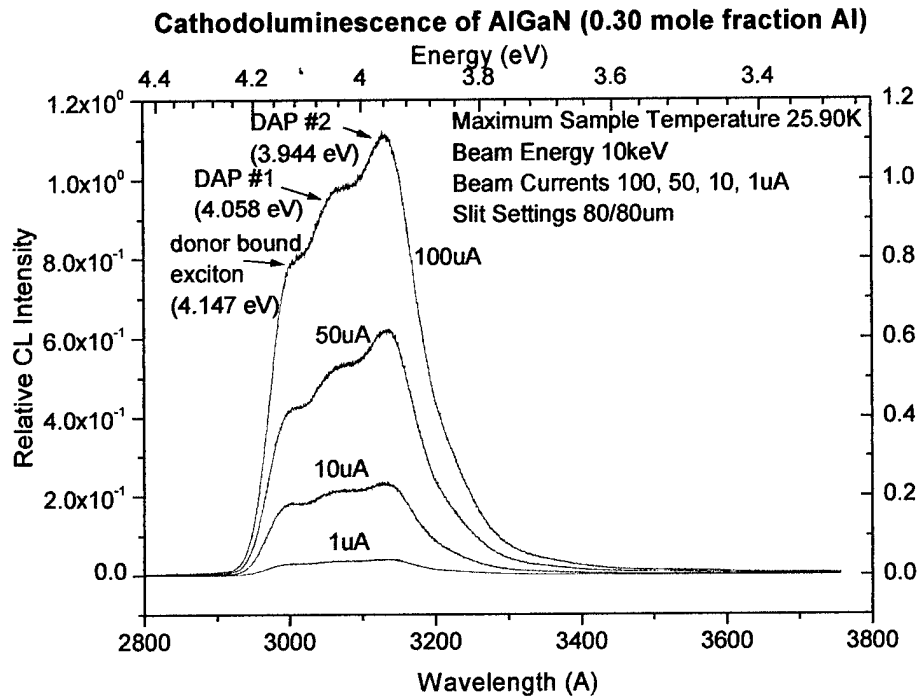


**Figure 4-8.** Cathodoluminescence of AlGaN ( $x = 0.30$ ) at constant beam energy

As mentioned earlier in this section, PeakFit was the program used as an aid to distinguish the peaks that make up the spectrum. Figures 4-10 and 4-11 show two examples of this program's output. The top figure is for the AlGaN ( $x = 0.20$ ) sample and the bottom is the AlGaN ( $x = 0.30$ ) sample. The plots consist of two sections. The top section shows the spectrum with the best fit curve, which is the summation of the peaks that are shown in the bottom section of the plot. The bottom section of the graph shows the decomposition of the spectrum into various peaks with the energy of each peak labeled. PeakFit was used to decompose all spectra taken.

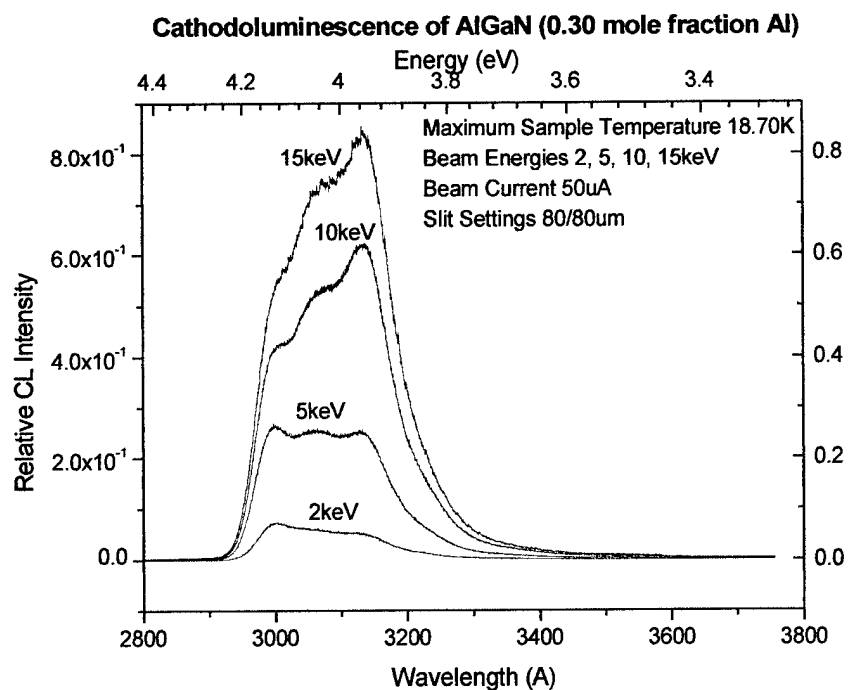
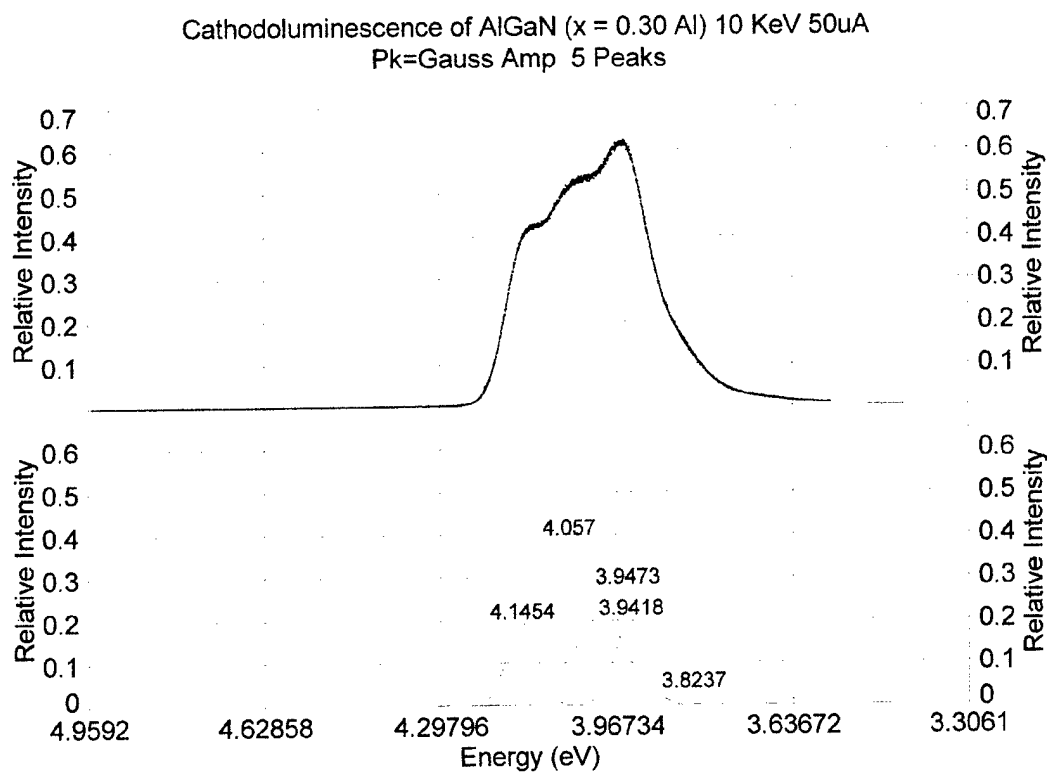
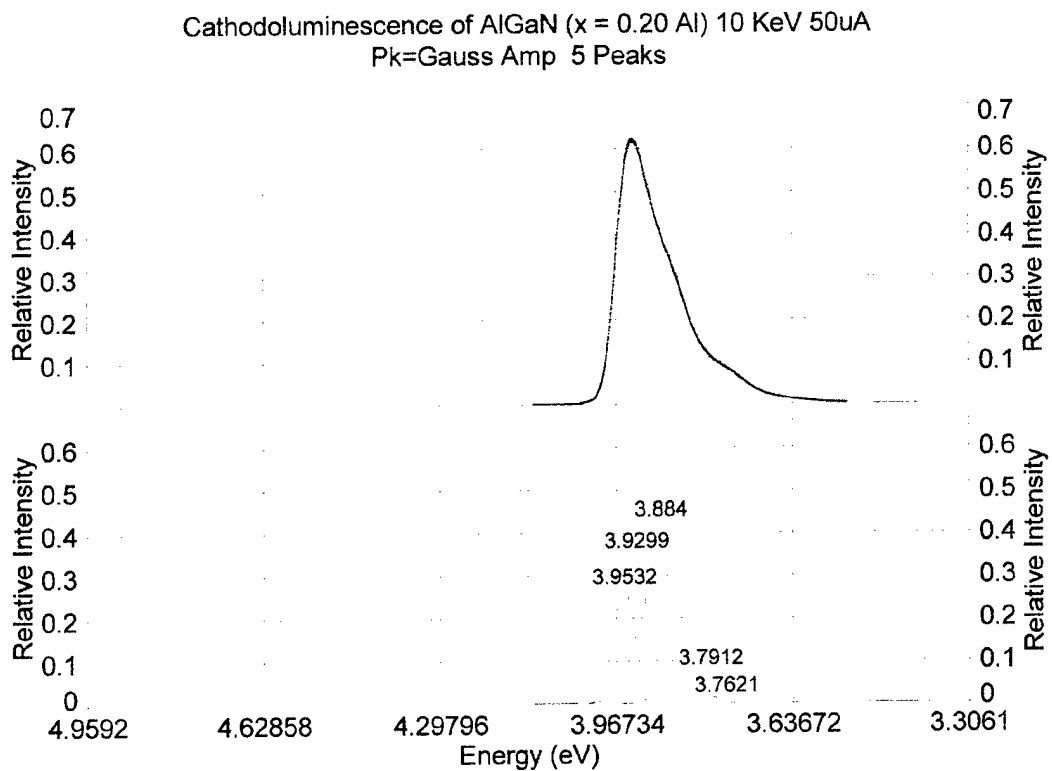


**Figure 4-9.** Cathodoluminescence of AlGa<sub>0.30</sub>N ( $x = 0.30$ ) at constant beam current

**TABLE 4-4**

Probable Transition Energies for Al<sub>*x*</sub>Ga<sub>1-*x*</sub>N

Transitions	Al <sub>0.10</sub> Ga <sub>0.90</sub> N	Al <sub>0.20</sub> Ga <sub>0.80</sub> N	Al <sub>0.30</sub> Ga <sub>0.70</sub> N	Al <sub>0.40</sub> Ga <sub>0.60</sub> N	Al <sub>0.50</sub> Ga <sub>0.50</sub> N
Donor bound exciton	3.684 eV (3365 Å)	3.953 eV (3136 Å)	4.147 eV (2989 Å)	4.182 eV (2964 Å)	4.170 eV (2973 Å)
DAP #1	3.668 eV (3380 Å)	3.884 eV (3192 Å)	4.058 eV (3055 Å)	4.074 eV (3043 Å)	3.986 eV (3110 Å)
DAP #2	N/A	3.791 eV (3270 Å)	3.944 eV (3143 Å)	3.983 eV (3112 Å)	3.821 eV (3244 Å)



Figures 4-10 & 4-11. PeakFit curves for AlGa<sub>N</sub> (x = 0.20 Al & x = 0.30 Al)

Table 4-5 lists the theoretical and the experimental band gap energies from CL and PL for the five AlGa<sub>N</sub> samples and the GaN standard. The theoretical values for ~ 5 K were calculated from equation (9). Using a band gap energy for AlN of 6.28 eV at 5 K and a band gap energy for GaN of 3.50 eV at 1.6 K (12:1378).

The values in Table 4-5 indicate that the AlGa<sub>N</sub> samples grown have mole fractions of aluminum different from the grower's specification. The theoretical band gap energies were calculated using equation (9). The nominal 0.10 mole fraction of aluminum is closer to a mole fraction of 0.07. The probable mole fraction for the 0.20, 0.30, 0.40 and 0.50 are 0.16, 0.23, 0.24, and 0.24, respectively. If the samples were 0.10, 0.20, 0.30, 0.40, and 0.50 then the energies (wavelengths) should increase (decrease) almost linearly in equally spaced divisions, which they clearly do not.

**TABLE 4-5**

Theoretical and Experimental Band Gap Energies of GaN and AlGa<sub>N</sub> at ~ 10 K

<b><i>Material</i></b>	<b>Theoretical Band Gap Energy</b>	<b>CL Experimental Band Gap Energy</b>	<b>PL Experimental Band Gap Energy</b>
GaN	3.50 eV (3542 Å)	3.479 eV (3563 Å)	3.480 eV (3562 Å)
Al <sub>0.1</sub> Ga <sub>0.9</sub> N	3.778 eV (3281 Å)	3.696 eV (3353 Å)	3.693 eV (3357 Å)
Al <sub>0.2</sub> Ga <sub>0.8</sub> N	4.056 eV (3056 Å)	3.953 eV (3136 Å)	3.962 eV (3129 Å)
Al <sub>0.3</sub> Ga <sub>0.7</sub> N	4.334 eV (2860 Å)	4.147 eV (2989 Å)	4.134 eV (2999 Å)
Al <sub>0.4</sub> Ga <sub>0.6</sub> N	4.612 eV (2680 Å)	4.168 eV (2974 Å)	No PL performed
Al <sub>0.5</sub> Ga <sub>0.5</sub> N	4.890 eV (2535 Å)	4.171 eV (2972 Å)	No PL performed

### AlN Buffer Layer

Next, the AlN peaks for all AlGaIn samples were studied using CL at the different beam currents and energies. The spectra for these peaks were very consistent for all but one sample ( $x = 0.10$ ) although there were slight variations in the positions of the peaks or spectral shapes when run at the different beam energies and currents. Table 4-6 on page 41 lists the peak energies for 10 keV at 50  $\mu$ A for the five samples. There were a couple of interesting observations obtained from this data. First, the exciton is usually the highest energy peak. However, from the data for  $x = 0.20, 0.30, 0.40,$  and  $0.50$  samples, the closest to the theoretical AlN energy (6.28 eV) is the third highest energy peak. A second observation is that the peak seen around 5.8 eV occurred in four of these samples (see Figures 4-12 and 4-13). The nature of this peak is unknown but was consistent in the four samples. However, the AlN peak for the  $x = 0.10$  sample is shifted by almost a 100 Å (see Figures 4-14 and 4-15) and the shape of the peak was significantly different from that observed in the other four samples. A possible explanation for this difference is the growth process. This sample was the only one grown on that particular day and was the first to be grown of the five. Therefore, some variation may have occurred during the AlN buffer layer growth on that day versus the following days on which the other samples were grown.

Note that the peak maximum in Figure 4-14 for 15 keV has shifted. A plausible explanation for this shift in the dominant peak was that the electron beam had penetrated into the substrate. Thus, the substrate may be affecting the luminescence of the sample. The width of the spectra increased from 150,



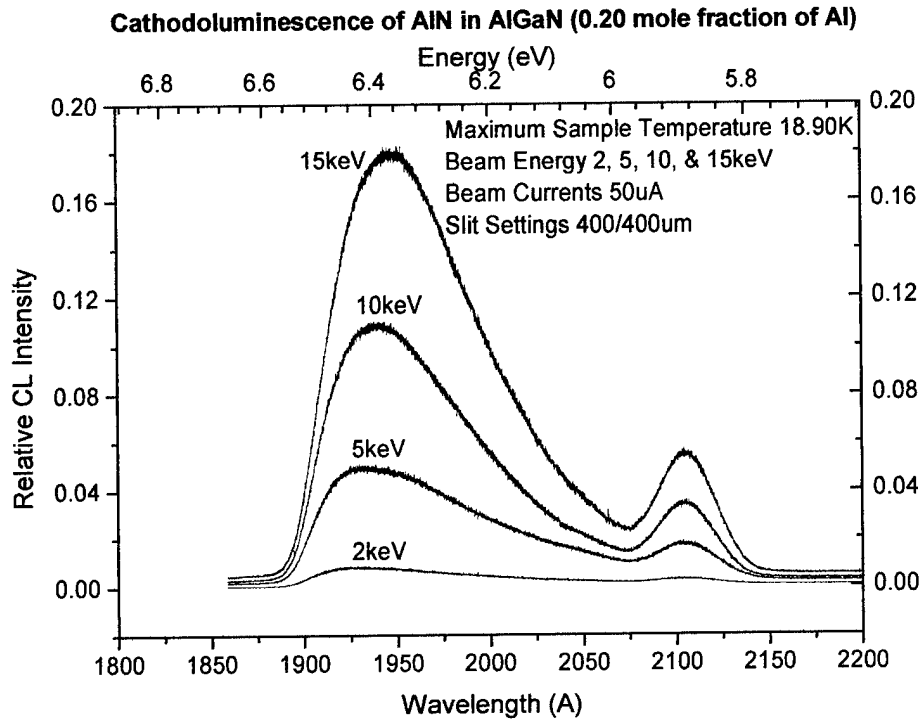


**Figure 4-12.** Cathodoluminescence of AlN in AlGa<sub>N</sub> ( $x = 0.20$ ) at constant beam current

275, 300, 350, and 350 Å for  $x = 0.10, 0.20, 0.30, 0.40$ , and  $0.50$ , respectively.

This agrees with the assumption that as the aluminum concentration increases it was oxidized by the extrinsic oxygen present. Recall that the nitrogen source or the dissociation of the sapphire wafer supplies the extrinsic oxygen. Thus, oxygen impurities were a probable rationale for the peak broadening.

The band gap energy for AlN at 5 K is approximately 6.28 eV (12:1378). The temperature of the samples during the experiment was about 10 K. Thus, it was feasible to make the assumption that the AlN band gap energy should be approximately 6.28 eV for the samples. Even at the lower beam energies where electron penetration remains within the epilayer of AlGa<sub>N</sub>, the AlN peak is still

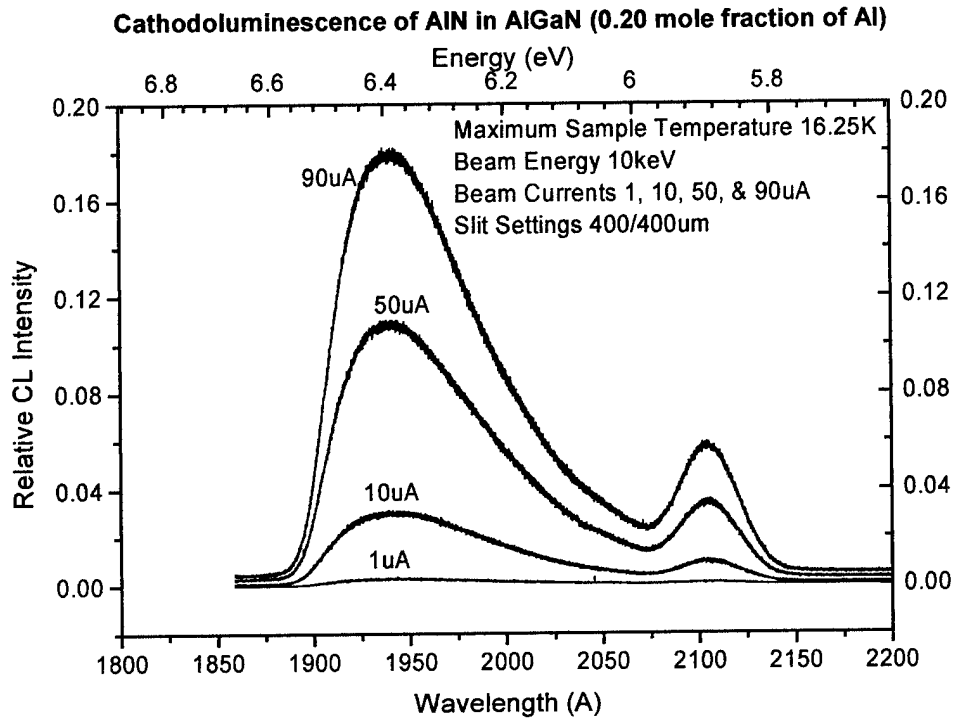


**Figure 4-13.** Cathodoluminescence of AlN in AlGaN ( $x = 0.20$ ) at constant energy

seen. Electrons can be generated at several locations in the material but radiative recombination mostly occurs in the AlGaN layer at lower beam energies.

However, the nitride layers are conducting, which allows the electrons to meander through the structure. Defects and large density dislocations at the interface of the sapphire substrate and epilayer can cause carrier trapping and recombination. This carrier trapping and recombination can lead to the luminescence of the AlN layer at these lower energies (21:3122).

**TABLE 4-6**

Peak Energies of AlN Buffer Layer

Transitions	$\text{Al}_{0.10}\text{Ga}_{0.90}\text{N}$	$\text{Al}_{0.20}\text{Ga}_{0.80}\text{N}$	$\text{Al}_{0.30}\text{Ga}_{0.70}\text{N}$	$\text{Al}_{0.40}\text{Ga}_{0.60}\text{N}$	$\text{Al}_{0.50}\text{Ga}_{0.50}\text{N}$
Peak #1	6.116 eV (2027 Å)	6.469 eV (1916 Å)	6.462 eV (1918 Å)	6.491 eV (1910 Å)	6.453 eV (1921 Å)
Peak #2	6.067 eV (2043 Å)	6.394 eV (1939 Å)	6.373 eV (1945 Å)	6.476 eV (1914 Å)	6.367 eV (1947 Å)
Peak #3	5.975 eV (2047 Å)	6.289 eV (1971 Å)	6.276 eV (1975 Å)	6.394 eV (1939 Å)	6.259 eV (1980 Å)
Peak #4	Not observed	5.886 eV (2106 Å)	5.879 eV (2108 Å)	5.892 eV (2104 Å)	5.895 eV (2103 Å)

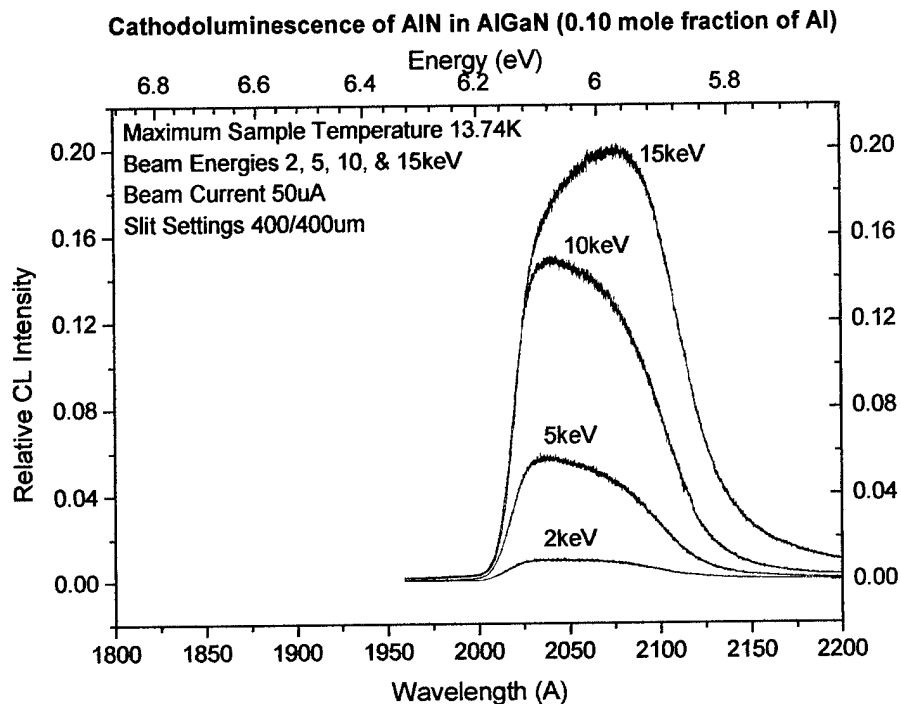


**Figure 4-14.** Cathodoluminescence of AlN in AlGa<sub>N</sub> ( $x = 0.10$ ) at constant beam current

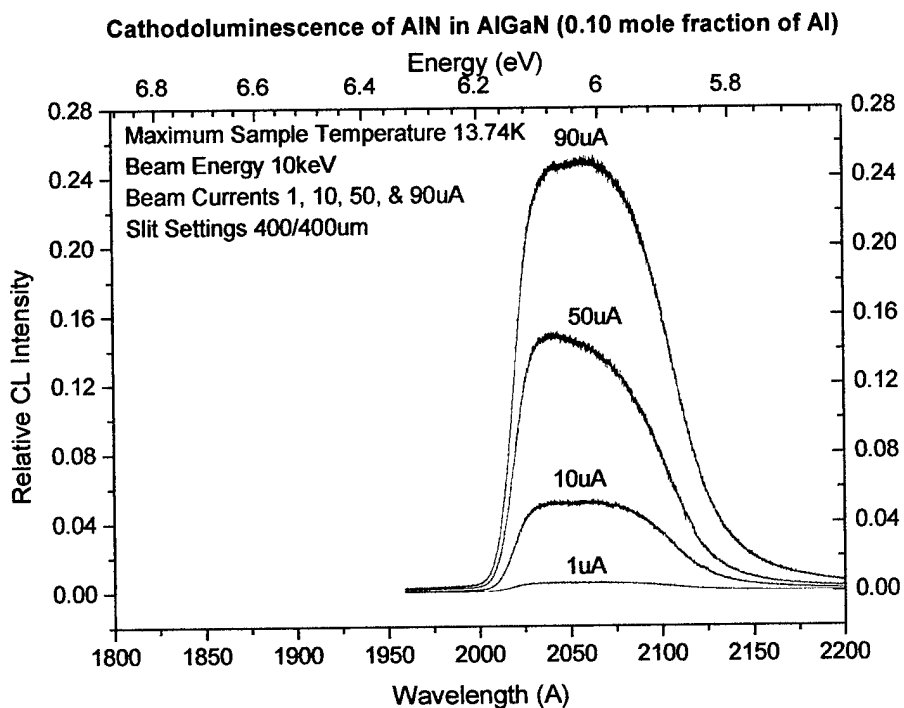


**Figure 4-15.** Cathodoluminescence of AlN in AlGa<sub>N</sub> ( $x = 0.10$ ) at constant beam energy

### Photoluminescence

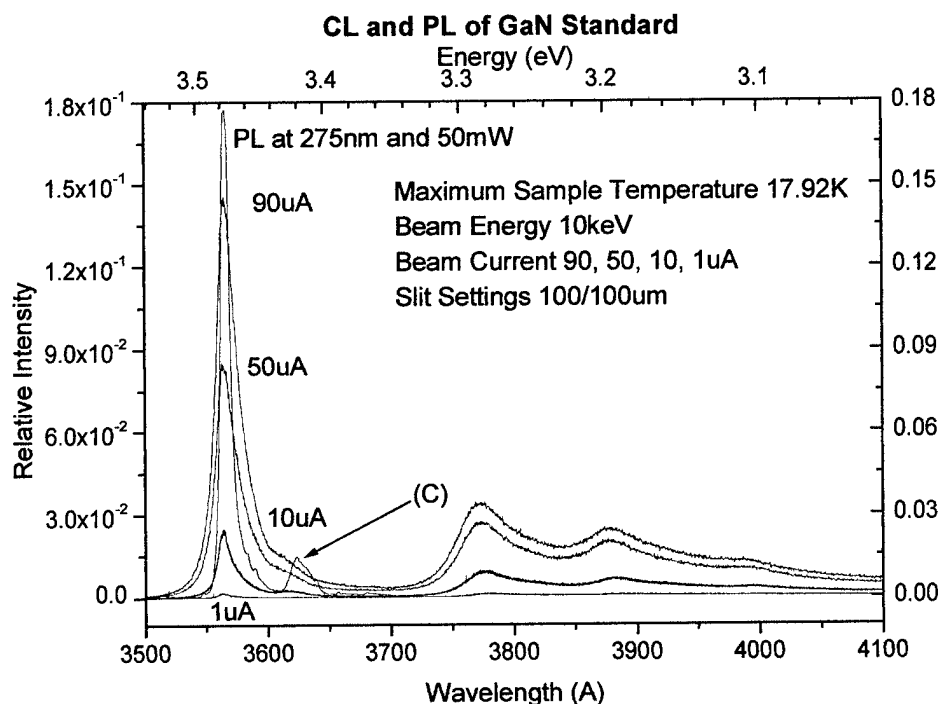
PL was performed on four of the six samples in an attempt to observe the shift in the position of the DAP transitions that was not observed in any of the CL data. The four samples examined were the GaN standard and AlGa<sub>N</sub> mole fraction of aluminum of  $x = 0.10$ ,  $x = 0.20$ , and  $x = 0.30$ . The DAP transition is characterized by a shift in the associated peak of about 100 Å (0.110 eV) with increased intensity. CL plots of different intensities were plotted with the PL data. The laser penetration depths were obtained using equation (7) and the absorption coefficients listed in Table 4-7 (17:214). This demonstrates that the excitation of electrons was occurring in the AlGa<sub>N</sub> layer during the PL experiment.

**TABLE 4-7**

Laser Penetration Depths

Material	Absorption Coefficient	Laser Penetration Depth
GaN	$7 \times 10^4 \text{ cm}^{-1}$	0.142 $\mu\text{m}$
Al <sub>0.11</sub> Ga <sub>0.89</sub> N	$8 \times 10^4 \text{ cm}^{-1}$	0.125 $\mu\text{m}$
Al <sub>0.20</sub> Ga <sub>0.80</sub> N	$8 \times 10^4 \text{ cm}^{-1}$	0.125 $\mu\text{m}$
Al <sub>0.38</sub> Ga <sub>0.62</sub> N	$8 \times 10^4 \text{ cm}^{-1}$	0.125 $\mu\text{m}$

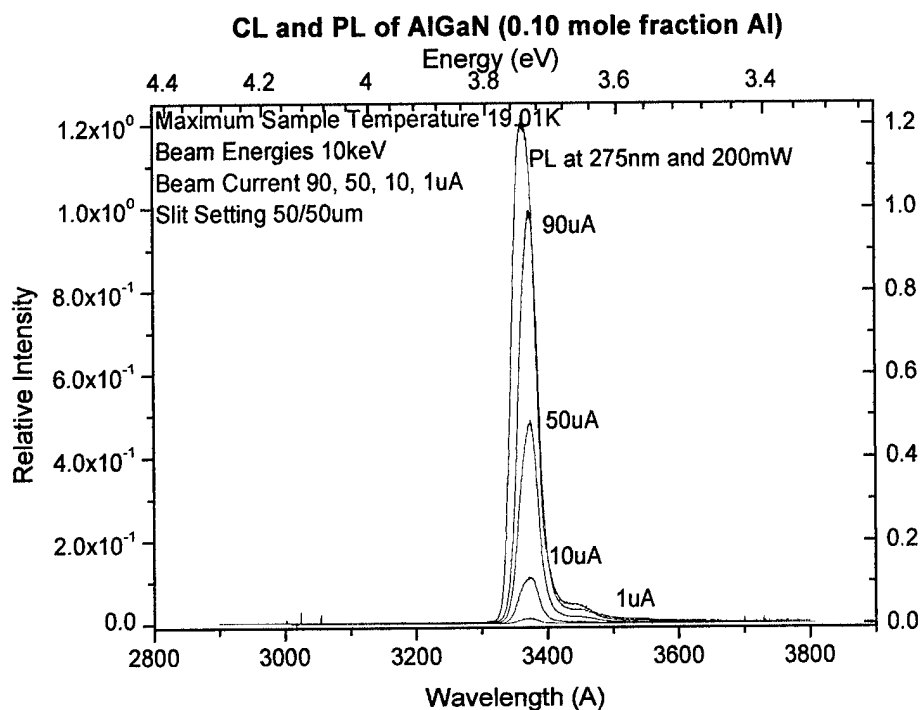
PL for the GaN standard was performed. The plot for PL is shown in Figure 4-16 graphed against the different intensities examined in the CL study. The peak positions for PL shift minutely as compared to the CL data. Also, notice that the shoulder in CL at about 3.428 eV is more distinguishable in the PL indicated by the label (C) at 3.418 eV. This shoulder is probably a shallow donor or acceptor peak possibly due to oxygen. The DAP shift was not observed.



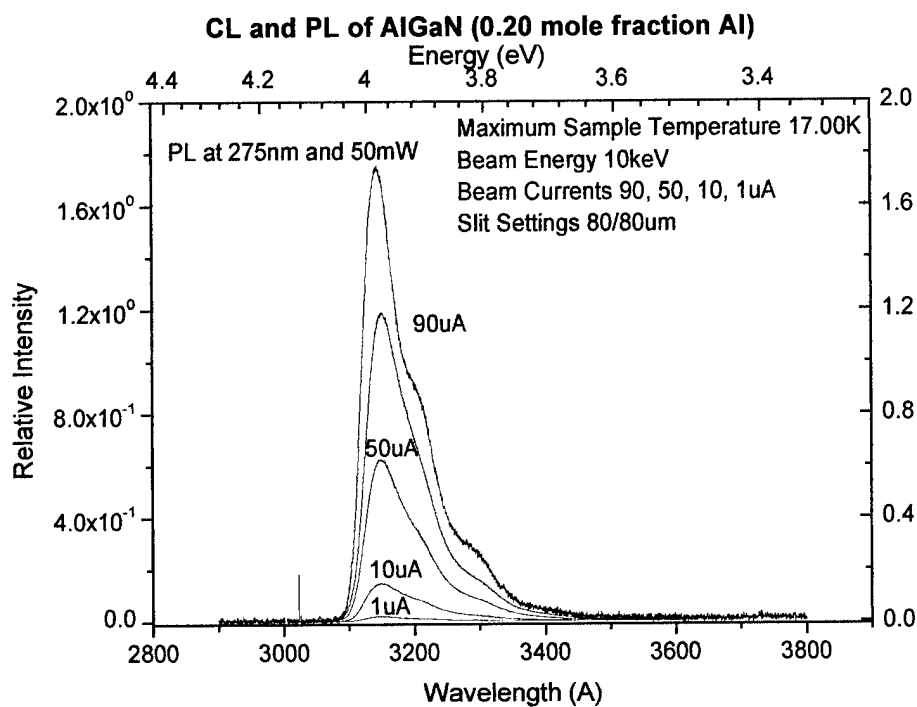
**Figure 4-16.** CL and PL spectra for GaN standard

Figure 4-17 is a plot of the CL spectra at different intensities for  $\text{Al}_{0.10}\text{Ga}_{0.90}\text{N}$ . Overlaid on this plot is the PL plot of this sample. From the plot, the positions of the peaks observed in the CL and PL data are in agreement with some variations in peak position. However, there is not a significant peak shift that would be associated with DAPs. The CL and PL spectra are similar in shape, position, and width.

The spectra for  $\text{Al}_{0.20}\text{Ga}_{0.80}\text{N}$  are shown in Figure 4-18. As in the previous spectra, the shape, position, and width differ slightly between the CL and PL spectra. There are slight shifts in the peak positions between the CL and PL data. As seen in the plot, the PL spectra peaks are easier to distinguish than in the CL. But again, the characteristic peak shift due to DAPs was not observed.



**Figure 4-17.** CL and PL spectra of AlGaN ( $x = 0.10$ )



**Figure 4-18.** CL and PL spectra of AlGaN ( $x = 0.20$ )

Next, the CL and PL of  $\text{Al}_{0.30}\text{Ga}_{0.70}\text{N}$  were examined. As before, slight changes in peak positions and spectrum width were observed between the CL and PL data. However, in this case the shape of the PL spectrum differs from the CL spectra. In the CL spectra, the bound exciton dominates at lower beam energies and the DAP #2 (oxygen) dominates at higher beam energies. In agreement with the CL data at higher beam energies, the PL shows the DAP #2 associated with oxygen as totally dominating the spectrum (see Figures 4-19 and 4-20). Lower powers of the laser were utilized and this DAP #2 at 0.50 mW at 275 nm was the only peak observed. The reason for the change in spectrum shape has not been determined. A possible explanation could be a localized oxygen impurity at the location examined in the PL experiment. As with the other samples, there was no DAP shift observed. Table 4-8 shows the PL transition energies. If you compare them to CL (see Table 4-8), there are some variations, which is probably due to errors in the experiment and determination of the peaks utilizing PeakFit.



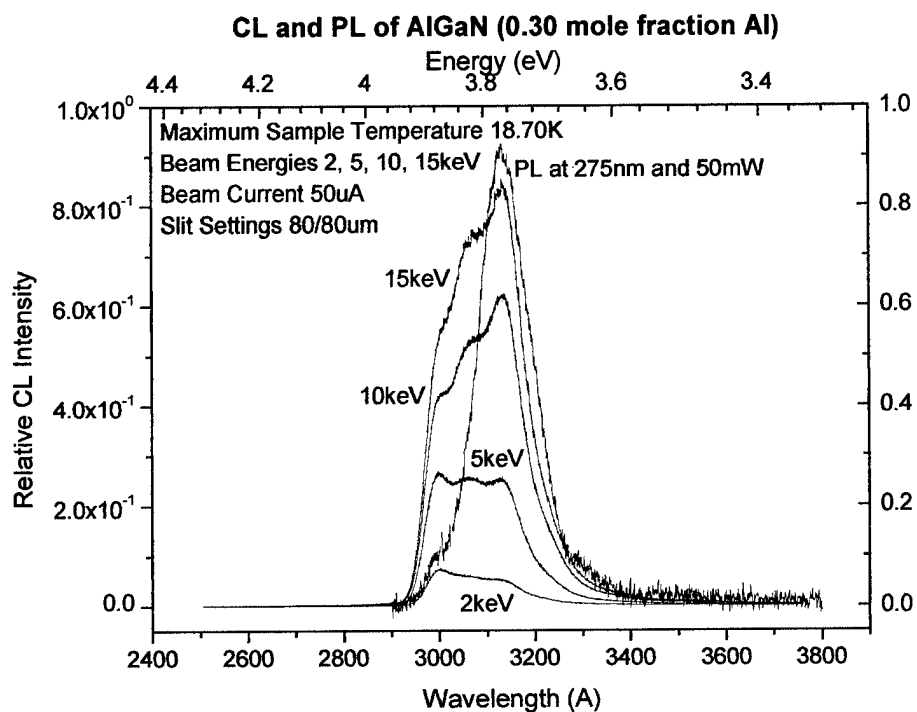


**Figure 4-19.** CL and PL spectra of AlGa<sub>N</sub> ( $x = 0.30$ ) at constant beam current

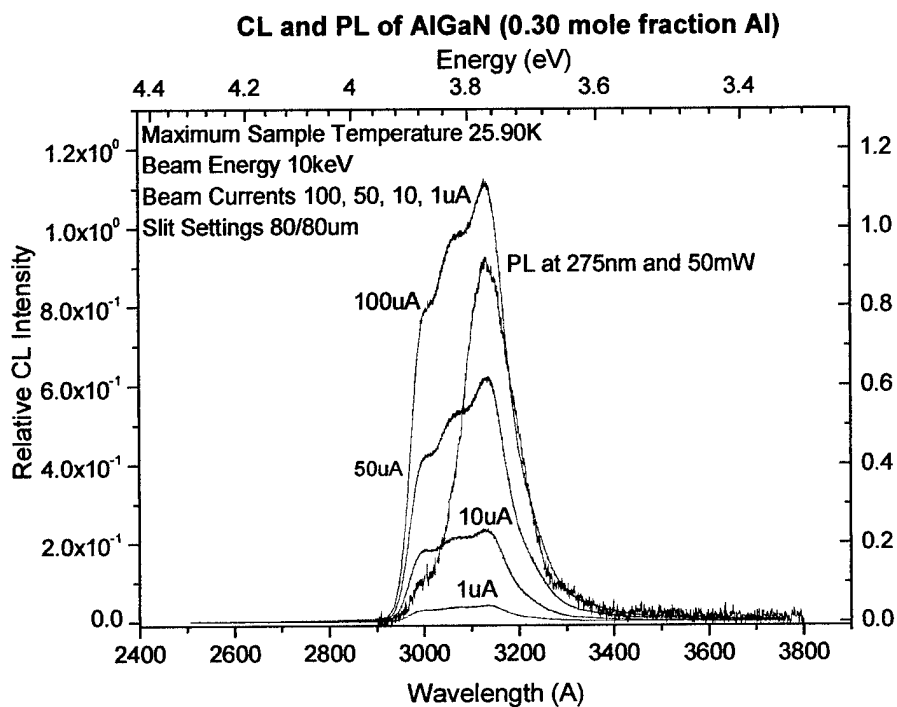


**Figure 4-21.** CL and PL spectra for AlGa<sub>N</sub> ( $x = 0.30$ ) at constant beam energy

**TABLE 4-8**

PL Transition Energies for GaN and AlGaN Samples

PL Settings	Transitions	GaN	$\text{Al}_{0.10}\text{Ga}_{0.90}\text{N}$	$\text{Al}_{0.20}\text{Ga}_{0.80}\text{N}$	$\text{Al}_{0.30}\text{Ga}_{0.70}\text{N}$
275 nm 0.50 mW	DAP #2	N/A	N/A	N/A	3.959 eV
275 nm 50 mW	Exciton	3.476 eV	N/A	3.962 eV	4.147 eV
	DAP #1			3.876 eV	4.074 eV
	DAP #2			3.798 eV	3.958 eV
275 nm 200 mW	Exciton	N/A	3.693 eV	N/A	4.134 eV
	DAP #1		3.672 eV		4.073 eV
	DAP #2				3.961 eV

## V. Conclusions and Recommendations

### Conclusions

As seen in the results and discussion chapter, there are discrepancies in the spectra from the samples studied. The implied aluminum mole fraction differs from that specified by the grower. This was seen when the experimental band gap values were compared to the theoretical values. This is particularly evident for samples with a mole fraction of  $x = 0.40$  and  $0.50$  which have band gap energies correlating more closely to  $x = 0.30$ . Therefore, the focus of this paper was on GaN,  $\text{Al}_{0.10}\text{Ga}_{0.90}\text{N}$ ,  $\text{Al}_{0.20}\text{Ga}_{0.80}\text{N}$ , and  $\text{Al}_{0.30}\text{Ga}_{0.70}\text{N}$ . The optical absorption data was found to be in agreement with the CL and PL data, and confirmed that the aluminum mole fractions were not correct. However, there were also differences in the band gap energies determined by optical absorption compared to those determined from CL and PL. These differences may be attributed to the fact that the cross section of the optical absorption light source on the samples was larger than the cross section of the electron or laser beams when positioned on the sample. Therefore, assuming a variation in composition over the sample, the optical absorption was more of an average of the sample's composition unlike CL and PL, whose spectra were collected at specific spots on the sample. Thus, to get a better idea of the uniformity of the aluminum composition, it would be advisable to try various spots on the sample using CL or PL. Time did not permit such a study as part of this thesis.

Disregarding the inaccuracy in composition, the samples with mole fractions of aluminum of  $x = 0.10$ ,  $0.20$ , and  $0.30$  are of suitable quality. Spectral shape and position of the peaks show little or no fluctuations in the CL data. The PL also supports this observation. However, the one exception to this observation is the  $x = 0.30$  sample. The

PL spectrum differs significantly in shape as compared to the CL. Curiously, the positions of the peaks of the spectrum correlate with the location of the peaks in CL. An explanation of this transformation in the shape is unknown at this time.

Certain information about defects and impurities were observed. Extrinsic oxygen impurities were a possible cause in the broadening of the spectra. As demonstrated by the data, the spectral width approximately triples from  $x = 0.10$  to  $0.30$ . As more aluminum, an oxygen getter, is added, the oxygen combines with it producing an impurity in the material. Thus, the higher aluminum content samples should have wider spectra. Also, structural defects due primarily from the lattice mismatch between sapphire and AlGaIn contribute to broadening of the spectra. The correction to this is to find a better lattice matched substrate to grow the material on. Research for a better substrate is currently in progress. Additional information about impurities and defects can be garnered from the DAPs peaks. This study attempted to observe the characteristic shift of the DAP peaks; however, none of the data verified this shift. A conceivable rationalization for not observing this shift was that it occurred at a higher or lower intensity than employed in either the CL or PL experiments.

The AlN peaks for the AlGaIn samples were investigated. The results were relatively similar for all the samples but one. The AlN peak for mole fraction of  $0.10$  was shifted to a lower energy as compared to the other four. The reason for this shift is unknown.

Finally, a large amount of data was collected and analyzed during this research. The findings were that the materials grown by MBE have not developed adequately to be utilized in semiconductor devices that require high quality. The major difficulty observed

was the inability to grow samples to the specified aluminum mole fraction. Once the composition uncertainty is solved, more effort can be applied to correcting the impurities and defects.

## Recommendations

The main focus of this research was to analyze the quality of MBE grown  $\text{Al}_x\text{Ga}_{1-x}\text{N}$  doped with silicon. The CL, PL, and optical absorption data correlate concerning the inaccuracy of aluminum concentration in the samples. However, the CL and PL band gap energies for the AlGa<sub>N</sub> samples differ from the band gap energies found in the optical absorption experiment. Recall that the band gap energy is an indicator of the aluminum mole fraction. Since there are variations in the data collected another method should be employed to determine the aluminum mole fraction. Secondary Ion Mass Spectroscopy (SIMS) or X-Ray Diffraction (XRD) has been utilized in the past to determine composition of  $\text{Al}_x\text{Ga}_{1-x}\text{N}$  (19:2). It is suggested that SIMS or XRD be employed to determine the composition of these materials. Another suggestion is to utilize CL or PL to make a map of the composition by running the experiment for various locations on the sample. This technique will give greater insight into uniformity, defects, and impurities as compared to examining the one locale. Additional analysis of the structural integrity of the sample can be determined through a multitude of techniques. Some of these technique applied in the past include Scanning Transmission Electron Microscopy (STEM), Atomic Force Microscopy (AFM), and High-Resolution X-Ray Diffraction (HRXRD) (1:13, 3:1). Since the samples were heavily doped with silicon, Hall measurements should be performed to determine the degree to which the silicon was activated. Lastly, an aim of this research was to identify DAPs. Since no characteristic shift occurred in any of the CL or PL data, a time-resolved experiment using a pulsed laser and the appropriate data collecting equipment is advised to try to distinguish the DAP transitions.

## Appendix A

This appendix expands on the discussion of penetration depth of the electron beam into the sample given in the main body of the thesis. The atomic number and molecular weights were taken from the periodic table. The density of AlN and GaN were found in CRC Handbook of Chemistry & Physics (11:12-97).

**TABLE A-1**

Periodic Properties of Aluminum, Gallium, and Nitrogen

<i>Periodic Table Property</i>	<b>Aluminum</b>	<b>Gallium</b>	<b>Nitrogen</b>
atomic number	13	31	7
molecular weight (gmole <sup>-1</sup> )	26.98	69.72	14.01

**TABLE A-2**

Density of AlN and GaN

<i>Property</i>	<b>AlN</b>	<b>GaN</b>
density (gcm <sup>-3</sup> )	3.26	6.10

The maximum depth of the electron beam penetration into the structure can be determined by Kanaya-Okayama equation (22:58)

$$R = [0.0276A/(Z^{0.89}\rho)]E_0^{1.67}$$

where

R = maximum depth of the electron beam  
penetration in  $\mu\text{m}$

A = atomic weight in gmole<sup>-1</sup>

Z = atomic number

$\rho$  = density in gcm<sup>-3</sup>

E<sub>0</sub> = incident electron beam energy in keV.

Table A-3 shows the different electron depth penetrations for the material examined in this research.

**TABLE A-3**

Electron Penetration Depths for GaN and AlGaN

<b><i>Material</i></b>	<b>Electron depth penetration at 2 keV</b>	<b>Electron depth penetration at 5 keV</b>	<b>Electron depth penetration at 10 keV</b>	<b>Electron depth penetration at 15 keV</b>
GaN	0.0439	0.203	0.646	1.272
Al <sub>0.1</sub> Ga <sub>0.9</sub> N	0.0457	0.211	0.672	1.322
Al <sub>0.2</sub> Ga <sub>0.8</sub> N	0.0476	0.220	0.699	1.377
Al <sub>0.3</sub> Ga <sub>0.7</sub> N	0.0496	0.229	0.729	1.436
Al <sub>0.4</sub> Ga <sub>0.6</sub> N	0.0519	0.240	0.762	1.500
Al <sub>0.5</sub> Ga <sub>0.5</sub> N	0.0543	0.251	0.798	1.571



## Appendix B

This appendix presents the plots for the AlGa<sub>N</sub> samples with an aluminum mole fractions of  $x = 0.40$  and  $x = 0.50$ . There are two plots for each of these samples. The first plot is constant beam energy followed by constant beam current for the CL study. The constant beam energy plots show the probable exciton and DAP peaks for each of the samples. Recall that PeakFit aided in decomposing the spectra into the various peaks.

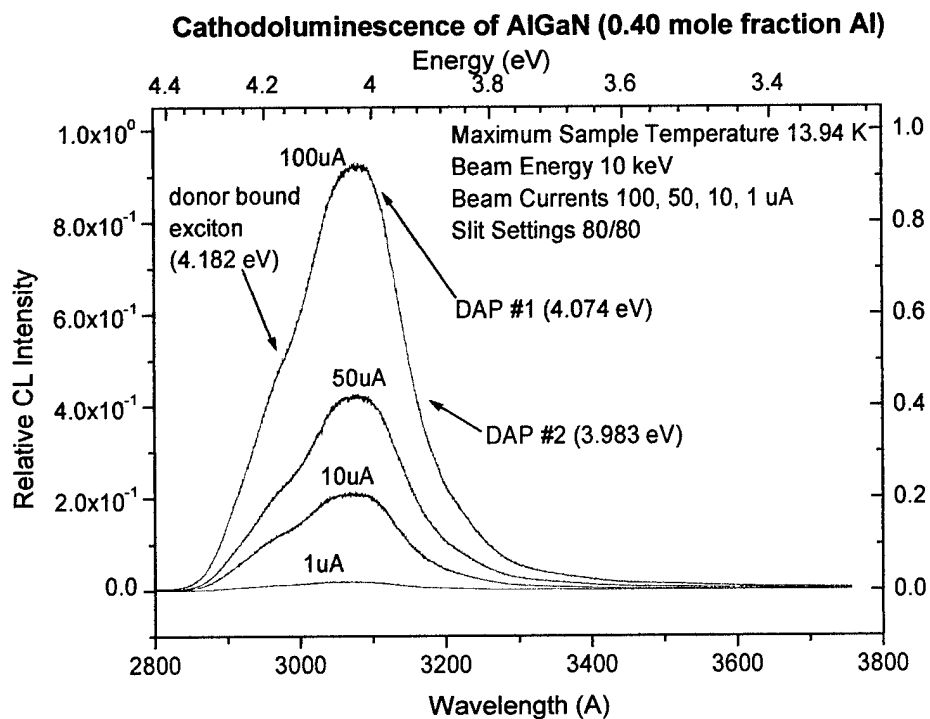


**Figure B-1.** Cathodoluminescence of AlGa<sub>N</sub> ( $x = 0.40$ ) at constant beam energy

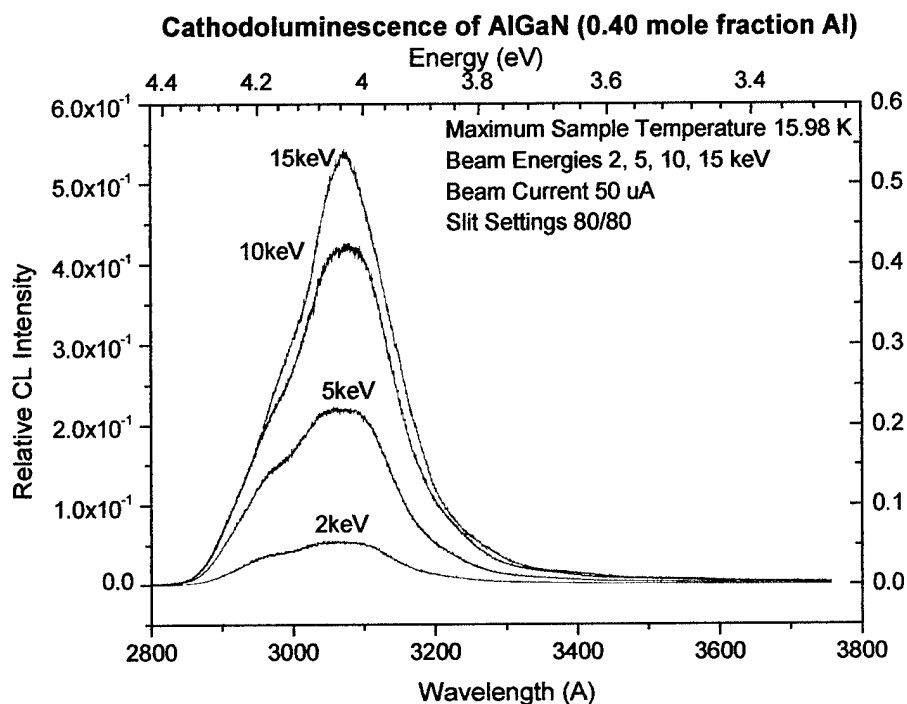


**Figure B-2.** Cathodoluminescence of AlGa<sub>N</sub> ( $x = 0.40$ ) at constant beam current

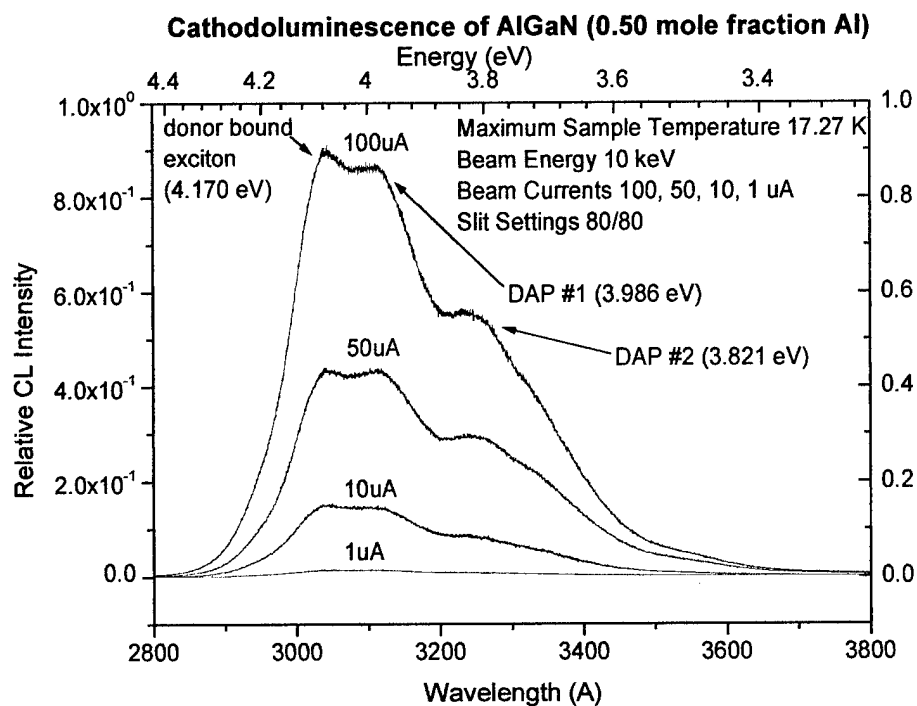


**Figure B-3.** Cathodoluminescence of AlGa<sub>N</sub> ( $x = 0.50$ ) at constant beam energy

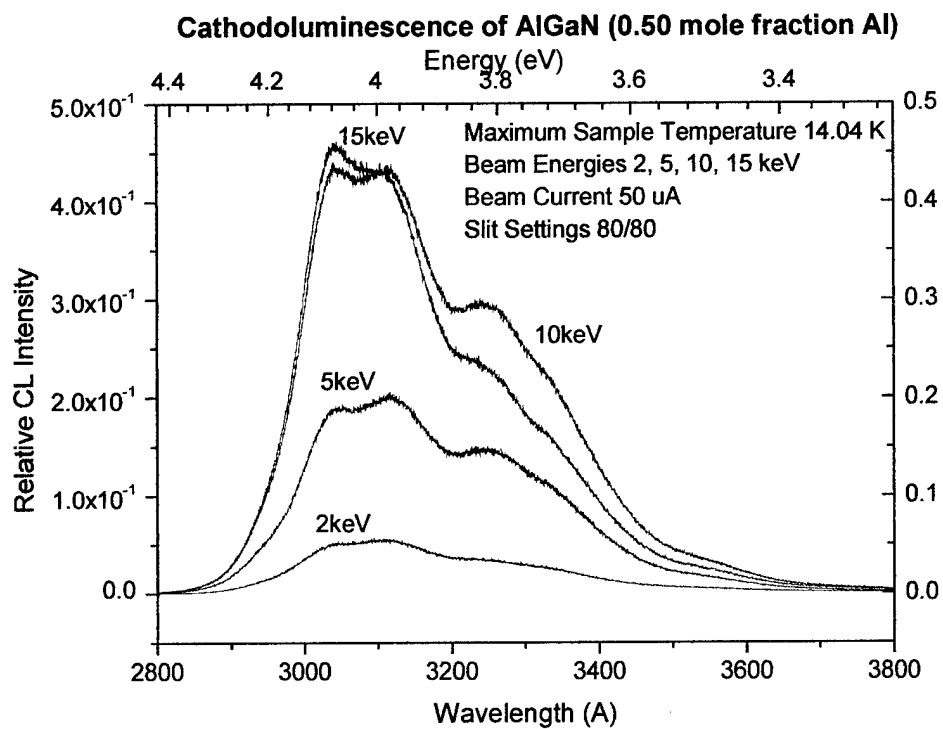


**Figure B-4.** Cathodoluminescence of AlGa<sub>0.50</sub>N ( $x = 0.50$ ) at constant beam current

## Bibliography

1. Chao, L. L., G. S. Cargill III, C. Kothandaraman, D. Cyr, G. Flynn, E. S. Hellman, D. Wiesmann, D. N. E. Buchanan, and I. Brener. "Nonuniform Morphology and Luminescence Properties of a Molecular Beam Epitaxy GaN Film from Atomic Force Microscopy, Scanning Electron Microscopy and Cathodoluminescence." <http://nsr.mij.mrs.org/2/7/test.html>. 1997.
2. DeForest, Daniel L. Cathodoluminescence and Photoluminescence Study of Silicon Implanted Gallium Arsenide. MS thesis, AFIT/GNE/PH/ 82M-6. Air Force Institute of Technology (AU), Wright-Patterson AFB OH, March 1982.
3. Dimitrov, R., L. Wittmer, H. P. Felsi, A. Mitchell, O. Ambacher, and M. Stutzmann. "Carrier Confinement in AlGaIn/GaN Heterostructures Grown by Plasma Induced Molecular Beam Epitaxy." <http://www.wileyvch.de/berlin/journals/pss/rapid/contents/98-030/dimitrov.html>. 27 July 1998.
4. Edgar, James H. "Properties of Group III Nitrides." Kansas State University: INSPEC, 1994.
5. "Effect of internal absorption on cathodoluminescence from GaN." <http://nsr.mij.mrs.org/3/4/test.html>. 1998.
6. "Fabrication and Characterization of GaN/AlGaIn Ultraviolet-band Heterojunction Photodiodes." <http://nsr.mij.mrs.org/3/7/test.html>. 1998.
7. Gregg, Michael R. Cathodoluminescence Spectroscopy of Zinc Germanium Phosphide. MS thesis, AFIT/GEP/ENP/92D. Air Force Institute of Technology (AU), Wright-Patterson AFB OH, December 1992.
8. "Growth and Doping of AlGaIn Alloys by ECR-assisted MBE." <http://nsr.mij.mrs.org/1/10/text.html>. 1996-1998.
9. Kanaya, K. and S. Okayama. "Penetration and energy-loss theory of electrons in solid targets." *Applied Physics Letters*, 5: 43-58. 1972.
10. Lakner, H., Q. Liu, G. Brockt, A. Radefeld, A. Meinert, and F. Scholz. "Investigation of inhomogeneities in (Al, Ga, In)N heterostructures by STEM and cathodoluminescence." *Material Science and Engineering*, B51: 44-52. 27 Feb 1998.
11. Lide, D. R., CRC Handbook of Chemistry and Physics 76<sup>th</sup> Edition. Florida: CRC Press, Inc., 1992.

12. Morkoc, H., S. Strite, G. B. Gao, M. E. Lin, B. Sverdlov, and M. Burns. "Large-band-gap SiC, III-V nitride, and II-VI ZnSe-based semiconductor device technologies." *Journal of Applied Physics*, 76 (3): 1363-1398. 1 Aug 1994.
13. "Optical Properties of Nitride-based Structures Grown on 6H-SiC." <http://nsr.mij.mrs.org/1/35/test.html>. 1996-1999.
14. Robins, L. H., and D. K. Wickenden. "Spatially resolved luminescence studies of defects and stress in aluminum gallium nitride films." *Applied Physics Letters*, 71: 3841-3843. 29 Dec 97.
15. Shan, W., J. W. Ager III, K. M. Yu, W. Walukiewicz, E. E. Haller, M. C. Martin, W. R. McKinney, and W. Yang. "Dependence of the fundamental band gap of  $\text{Al}_x\text{Ga}_{1-x}\text{N}$  on alloy composition and pressure." *Journal of Applied Physics*, 85 (12): 8505-8507. 11 Mar 1999.
16. Silkowski, Eric. Luminescence Study of Ion Implanted GaN. Doctoral Dissertation, Air Force Institute of Technology (AU), Wright-Patterson AFB OH, November 1996.
17. Stutzmann, M., O. Ambacher, A. Cros, M. S. Brandt, H. Angerer, R. Dimitrov, N. Reinacher, T. Metzger, R. Hopler, D. Brunner, F. Freudenberg, R. Handschuh, and Ch. Deger. "Properties and applications of MBE grown AlGaIn." *Material Science and Engineering*, B50: 212-218. 18 Dec 1997.
18. Sze, S. M. Semiconductor Devices Physics and Technology. New York: John Wiley & Sons., 1985.
19. "Temperature-Composition Dependence of the Bandgap and Possible Non-coplanar Structures in GaN-AlN, GaN-InN and InN-AlN Mixed Crystals." <http://nsr.mij.mrs.org/2/3/test.html>. 1997.
20. Van Nostrand, J. E., J. Solomon, A. Saxler, Q. -H. Xie, D. C. Reynolds, and D. C. Look. "Dissociation of  $\text{Al}_2\text{O}_3(0001)$  substrates, and the roles of silicon and oxygen in n-type GaN thin solid films grown by gas-source molecular beam epitaxy."
21. Van Nostrand, J. E., R. L. Hengehold, K. D. Leedy, J. T. Grant, J. L. Brown, and Q.-H. Xie. "Cathodoluminescence, microstructure, and morphology of tensile-strained  $\text{Al}_x\text{Ga}_{(1-x)}\text{N}$  epitaxial films grown by gas source molecular beam epitaxy." *Journal of Applied Physics*, 86 (6): 3120-3127. 15 Sep 1999.
22. Yacobi, B. G., and D. B. Holt. Cathodoluminescence Microscopy of Inorganic Solids. New York: Plenum Press, 1990.

23. Zubrilov, A. S., D. V. Tsvetkov, V. I. Nikolaev, and I. P. Nikitina. "Edge luminescence of AlN-GaN solid solutions." *Semiconductors*, 30 (11): 1069-1073. Nov 1996.

## **Vita**

Judith Lorraine McFall was born on January 15, 1971 in Binghamton, New York. She received her Diploma from Whitney Point High School, a small village school north of Binghamton, New York, in June 1989. In the fall of 1989, she began her education in the aviation forum at Embry-Riddle Aeronautical University in Daytona Beach, Florida. Five years later, she obtained her Bachelor of Science in Aerospace Engineering. Also, she graduated with a FAA private pilot and aircraft dispatch license. She returned to New York, where she worked for BFGoodrich Aerospace for two years in the aircraft electrical harness section. On January 8, 1997, she entered Officers Training School at Maxwell Air Force Base. She was commissioned on April 18, 1997, and sent to 6th Space Operations Squadron at Offutt Air Force Base, Nebraska. There she was a hardware engineer on the Defense Meteorological Satellite Program for about a year and a half. Finally, she was accepted into the Physics Department at AFIT to obtain a masters in Material Science and Engineering.

<b>REPORT DOCUMENTATION PAGE</b>			Form Approved OMB No. 074-0188	
Public reporting burden for this collection of information is estimated to average 1 hour per response, including the time for reviewing instructions, searching existing data sources, gathering and maintaining the data needed, and completing and reviewing the collection of information. Send comments regarding this burden estimate or any other aspect of the collection of information, including suggestions for reducing this burden to Washington Headquarters Services, Directorate for Information Operations and Reports, 1215 Jefferson Davis Highway, Suite 1204, Arlington, VA 22202-4302, and to the Office of Management and Budget, Paperwork Reduction Project (0704-0188), Washington, DC 20503				
<b>1. AGENCY USE ONLY (Leave blank)</b>		<b>2. REPORT DATE</b> March 2000	<b>3. REPORT TYPE AND DATES COVERED</b> Master's Thesis	
<b>4. TITLE AND SUBTITLE</b>  OPTICAL INVESTIGATION OF MOLECULAR BEAM EPITAXY $\text{Al}_x\text{Ga}_{1-x}\text{N}$ TO DETERMINE MATERIAL QUALITY			<b>5. FUNDING NUMBERS</b>	
<b>6. AUTHOR(S)</b>  Judith L. McFall, First Lieutenant, USAF				
<b>7. PERFORMING ORGANIZATION NAME(S) AND ADDRESS(ES)</b>  Air Force Institute of Technology Graduate School of Engineering and Management (AFIT/EN) 2950 P Street, Building 640 WPAFB OH 45433-7765			<b>8. PERFORMING ORGANIZATION REPORT NUMBER</b>  AFIT/GMS/ENP/00M-01	
<b>9. SPONSORING / MONITORING AGENCY NAME(S) AND ADDRESS(ES)</b> AFRL/MLPA Attn: Joe E. Van Nostrand 2977 P Street STE #1 WPAFB OH 45433-7734 DSN: 785-2227 ext. 3389			<b>10. SPONSORING / MONITORING AGENCY REPORT NUMBER</b>	
<b>11. SUPPLEMENTARY NOTES</b>  Dr. Robert L. Hengehold, ENP, DSN: 785-3636 ext. 4502				
<b>12a. DISTRIBUTION / AVAILABILITY STATEMENT</b>  APPROVED FOR PUBLIC RELEASE; DISTRIBUTION UNLIMITED.			<b>12b. DISTRIBUTION CODE</b>	
<b>ABSTRACT (Maximum 200 Words)</b>  The purpose of this research was to determine the quality of AlGaIn samples with various mole fractions of aluminum doped with silicon. The samples utilized for this study were composed of an AlN buffer layer sandwiched between the sapphire substrate and AlGaIn epilayer grown by molecular beam epitaxy (MBE). Cathodoluminescence (CL) and photoluminescence (PL) were employed to determine the mole fraction of aluminum in each sample. These techniques also gave insight into the material's nonuniformity, defects, and impurities. CL was run at 4 different beam energies (2, 5, 10, & 15 keV) with four different currents (1, 10, 50, & 90 $\mu\text{A}$ ) for the GaN standard sample, AlGaIn samples, and AlN buffer layers in the AlGaIn samples. PL was also used to try to distinguish between certain transitions. Optical absorption was performed to obtain band gap energies to compare to those found in CL and PL.  The finding of this study was that AlGaIn grown by MBE is a good method for aluminum mole fractions of less than 0.30. Above this mole fraction, either a different growth technique or modifications to the MBE growth cycle are necessary to obtain quality material for semiconductor devices with applications in plume detection and threat warning systems.				
<b>14. SUBJECT TERMS</b> Semiconductors, Cathodoluminescence, Photoluminescence, Optical absorption, GaN, AlN buffer layer, AlGaIn			<b>15. NUMBER OF PAGES</b> 71	
			<b>16. PRICE CODE</b>	
<b>17. SECURITY CLASSIFICATION OF REPORT</b> UNCLASSIFIED	<b>18. SECURITY CLASSIFICATION OF THIS PAGE</b> UNCLASSIFIED	<b>19. SECURITY CLASSIFICATION OF ABSTRACT</b> UNCLASSIFIED	<b>20. LIMITATION OF ABSTRACT</b> UL	

NSN 7540-01-280-5500

Standard Form 298 (Rev. 2-89)  
Prescribed by ANSI Std. Z39-18  
298-102